



HAL
open science

Hydration state of the Martian surface as seen by Mars Express OMEGA: 1. Analysis of the 3 μ m hydration feature

D. Jouglet, F. Poulet, R. Milliken, J. Mustard, J.-p. Bibring, Y. Langevin, B. Gondet, Cécile Gomez

► To cite this version:

D. Jouglet, F. Poulet, R. Milliken, J. Mustard, J.-p. Bibring, et al.. Hydration state of the Martian surface as seen by Mars Express OMEGA: 1. Analysis of the 3 μ m hydration feature. *Journal of Geophysical Research. Planets*, 2007, 112 (E8), 10.1029/2006JE002846 . hal-04439190

HAL Id: hal-04439190

<https://hal.science/hal-04439190>

Submitted on 6 Feb 2024

HAL is a multi-disciplinary open access archive for the deposit and dissemination of scientific research documents, whether they are published or not. The documents may come from teaching and research institutions in France or abroad, or from public or private research centers.

L'archive ouverte pluridisciplinaire **HAL**, est destinée au dépôt et à la diffusion de documents scientifiques de niveau recherche, publiés ou non, émanant des établissements d'enseignement et de recherche français ou étrangers, des laboratoires publics ou privés.

Hydration state of the Martian surface as seen by Mars Express OMEGA:

1. Analysis of the 3 μm hydration feature

D. Jouglet,¹ F. Poulet,¹ R. E. Milliken,² J. F. Mustard,² J.-P. Bibring,¹ Y. Langevin,¹ B. Gondet,¹ and C. Gomez¹

Received 17 October 2006; revised 23 February 2007; accepted 29 May 2007; published 29 August 2007.

[1] Global mapping by the visible/near-infrared OMEGA spectrometer gives the first opportunity to study in detail the characteristics of the 3 μm hydration absorption on the surface of Mars. This feature is caused by bending and stretching vibrations of adsorbed or structural H₂O and/or OH⁻ bound to minerals. A specific data reduction scheme has been developed to remove the contribution of thermally emitted radiance from OMEGA spectra. With the derived albedo spectra, variations in strength and shape of the 3 μm feature can be accurately assessed. Calibration issues are discussed and data only within the nominal calibration level of the instrument are analyzed, which corresponds to a surface coverage of $\sim 30\%$. All OMEGA spectra exhibit the presence of this absorption feature, which can be explained by the presence of adsorbed water as well as by alteration rinds or coatings resulting from weathering. Strong variations of the band strength are observed. Correlations between hydration, albedo, and elevation are examined. Terrains enriched in phyllosilicates, sulfates, or hydroxides exhibit an increased hydration signature as well as a weaker combination overtone H₂O absorption at $\sim 1.9 \mu\text{m}$. Careful analysis also reveals seasonal variations in surface hydration, with soils in the northern midlatitudes decreasing in hydration between northern spring and summer. This hydration change is best explained by the presence of winter frost followed by equilibration of frost-free soil with the atmosphere and by increased surface temperatures reducing the adsorptive capacity of the regolith.

Citation: Jouglet, D., F. Poulet, R. E. Milliken, J. F. Mustard, J.-P. Bibring, Y. Langevin, B. Gondet, and C. Gomez (2007), Hydration state of the Martian surface as seen by Mars Express OMEGA: 1. Analysis of the 3 μm hydration feature, *J. Geophys. Res.*, 112, E08S06, doi:10.1029/2006JE002846.

1. Introduction

[2] The average Martian atmospheric pressure of 6 mbar and the low proportion of water vapor make liquid H₂O unstable on the surface over long timescales. Transient liquid water may occur for short durations [Richardson and Mischna, 2005; Hecht, 2002], while the presence of sub-surface liquid water reservoirs has not yet been detected [Picardi *et al.*, 2005]. Nevertheless, water is not absent on Mars and three reservoirs have been identified by probes and rovers: water ice at the poles as detected by Viking [Farmer *et al.*, 1976] and OMEGA [Bibring *et al.*, 2004b; Langevin *et al.*, 2005a], water vapor in the atmosphere [Titov, 2002; Smith, 2004], and H⁺ (assumed to be associated with H₂O or OH⁻ groups) in the upper layers (first meter) of the regolith [Feldman *et al.*, 2004].

Hydration of rocks and soils recently identified by orbital and ground instruments [Bibring *et al.*, 2005; Squyres *et al.*, 2004] could represent a major component of this last category. These reservoirs have the potential to exchange water over days, years and longer timescales, such that accurate numerical models of the global water cycle must account for all of them [Böttger *et al.*, 2005]. This paper focuses on the hydration of the Martian surface by examining data acquired by the near-infrared imaging spectrometer OMEGA (Observatoire pour la Minéralogie, l'Eau, les Glaces et l'Activité) on board the European Space Agency's Mars Express mission.

[3] After a review of the several forms of hydration that can exist on the Martian surface, the first part of the paper is focused on the methods for data reduction, including a detailed discussion of the instrumental calibration and the method for estimating the hydration through the 3 μm feature. We then present the results about hydration of the Martian surface and its variation with different parameters (albedo, composition, elevation and season). A companion paper [Milliken *et al.*, 2007] presents an analysis of the

¹Institut d'Astrophysique Spatiale (IAS), Université Paris 11, Orsay, France.

²Department of Geological Sciences, Brown University, Providence, Rhode Island, USA.

Martian surface water content based on laboratory measurements [Milliken and Mustard, 2005].

2. Background

[4] Several forms of hydration in minerals can exist on the surface of Mars (see Bruckenthal and Singer [1987], Cooper and Mustard [1999], and Richard et al. [2006] for reviews). Three main classes of H₂O are considered: surface adsorbed water, structurally adsorbed water, and structurally bound water. (1) Adsorbed water is a generic term to name all forms of fixation of water inside minerals that can exchange easily with surrounding air. Surface adsorbed water consists of one to a few layers of water molecules loosely bound to the external surface of grains. This fixation is due to Van der Waals interaction or H-bonds according to the following scheme: mineral-water-atmosphere. Minerals exhibiting microporosity can also adsorb water molecules on the surface of their micropores according to the stronger mineral-water-mineral scheme. (2) Hydration on Mars may also be structurally adsorbed water: some minerals have the capacity to store variable amounts of H₂O in specific inner sites, even under Mars surface conditions [Bish et al., 2003; Fialips et al., 2004; Vaniman et al., 2004]. Certain clay minerals, for example, store H₂O in their interlayer sites and zeolites can store H₂O inside their channels. Such structurally adsorbed water molecules may be linked to minerals over a wide range of energies, making some water molecules easy to remove by decreasing pressure or relative humidity and others difficult to remove even through heating [Milliken and Mustard, 2005]. Möhlmann [2004] showed that adsorbed water with low bond energies should play an important role in the Martian water cycle. (3) The third class of hydration is structurally bound water. It means water that is part of the crystal lattice of minerals and that cannot be removed without destroying the crystal. While the exchange of adsorbed water between minerals and ambient air is reversible and can occur over short timescales, structurally bound H₂O is strongly held and requires higher energies to be removed over relatively short timescales. This process is typically irreversible. Removing water trapped in glasses or OH⁻ in clay minerals, for instance, requires heat and destroys the structure of mineral. Bish et al. [2003] showed that strong hydration bonds in certain sulfates could be stable over billions of years and provide evidence for a past aqueous environment. The limit between these three classes is not strict, depending on bond energy and the kinetics of fixation/removal. (4) Finally the presence of structural OH linked to cations can also contribute to the strength of the 3 μm feature. Such metal-OH bonds are a very stable form of hydration. Other forms of hydration known to exist on Earth, for example capillarity water or bulk water inside macropores of minerals [Richard et al., 2006], are not considered because they have a liquid-like behavior and are unstable on Mars.

[5] Near-infrared reflectance spectroscopy of the Martian surface can provide a wealth of information about the presence of hydrated minerals within the uppermost fraction of the regolith. Hydration may be detected by the presence of absorption bands at 1.4 μm, 1.9 μm, in the 2.1–2.4 μm range, and at 3 μm [see Bibring et al., 2005]. These bands are due to the stretching and bending vibrations of the H₂O

molecule or the OH group. Bishop et al. [1994] present a review of the theoretical assignment of each band. The OMEGA instrument has detected the 1.4 μm, 1.9 μm, and the 2.1–2.4 μm hydration bands, and thus the presence of phyllosilicates and sulfates on Mars [Arvidson et al., 2005; Langevin et al., 2005b; Gendrin et al., 2005; Poulet et al., 2005a]. However, these specific hydrated minerals are observed only for a few places on the surface of Mars.

[6] Prior to the OMEGA results, two near-infrared spectrometers, IRS aboard Mariner 6 and 7 [Pimentel et al., 1974; Calvin, 1997] and ISM aboard Phobos [Bibring et al., 1989; Murchie et al., 1993], observed a broad and deep 3 μm absorption band in each spectrum, with variability in depth and shape. This band can influence reflectance spectra from ~2.7 to 4 μm. All forms of hydration influence the strength and shape of the 3 μm band, through fundamental symmetric and asymmetric H₂O stretches centered near ~2.9 μm, the overtone of the H₂O bend at ~3.1 μm, and the metal-OH stretch at 2.7 μm [Milliken and Mustard, 2005; Cooper and Mustard, 1999]. However, the absorption of metal-OH occurs within a strong atmospheric CO₂ absorption. Thus our evaluation of the 3 μm feature will focus on absorptions resulting mainly from the presence of H₂O. The study of this band with OMEGA data is consequently important to (1) identify the current form(s) of water responsible for this band, (2) better understand the relationship between the form of water and the associated alteration processes, and (3) get information about the interaction of minerals with the atmosphere, seasonal surface frost, and hydrogen reservoirs discovered by the Mars Odyssey Gamma Ray Spectrometer (GRS) suite of instruments.

[7] Several works have performed laboratory studies of the 3 μm absorption band. In particular, studies have tried to link the shape and depth of the 3 μm band with the type of mineral and the amount of water in these minerals. Yen et al. [1998] measured the apparent absorbance (negative natural logarithm of the reflectance) of several Martian-like samples with different water contents. More recently, Milliken and Mustard [2005] tested the accuracy of different band parameters to measure the strength of hydration bands and how they relate to the amount of water in the mineral. Cooper and Mustard [1999] examined the influence of grain size on hydration bands. Additionally, Zent and Quinn [1995, 1997] and Jänchen et al. [2006] provided important results regarding adsorption isotherms and isobars of water at equilibrium under Mars surface conditions.

[8] We examine the 3 μm band present in Martian soils by using data returned by the OMEGA near-infrared imaging spectrometer, which has been acquiring three-dimensional images (x, y, λ) since December 2003, corresponding to 370 million spectra ranging from 0.3 μm to 5.1 μm. Each spectrum represents an observation of a square on the surface with spatial range between 300 m and 5 km per pixel, depending on the altimetry of the Mars Express spacecraft [Bibring et al., 2004a]. Data are acquired from ~0.3 μm to 1.0 μm by the visible (V) channels, from 1.0 μm to 2.5 μm by the short wavelength infrared (SWIR-C) channels, and from 2.5 μm to 5.1 μm by the short wavelength infrared (SWIR-L) channels. Spectral sampling varies from 7 to 20 nm. From December 2003 to July 2006 OMEGA has covered ~80% of the surface

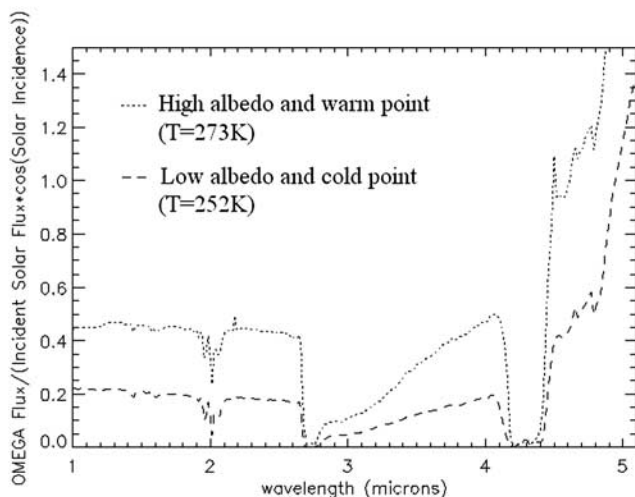


Figure 1. Light flux received by OMEGA from two points of Mars surface, divided by incident solar flux and corrected by Lambert's law. Dotted curve corresponds to a high albedo and hot point; dashed curve corresponds to a low albedo and less warm point. Between $2.6 \mu\text{m}$ to $2.9 \mu\text{m}$ and between $4.1 \mu\text{m}$ and $4.6 \mu\text{m}$, no data are available since the atmospheric absorption is total (Figure 2). These spectra also exhibit atmospheric bands at $2 \mu\text{m}$ and around $4.6 \mu\text{m}$.

at low spatial resolution (kilometers per pixel) and $\sim 10\%$ at high spatial resolution (hundreds of meters per pixel). To date, global studies using OMEGA data have been based only on the C channel. The L channel, however, is well suited to the global study surface hydration since the $3 \mu\text{m}$ feature occurs entirely within its wavelength range.

3. Data Reduction

[9] Data reduction, which consists in converting OMEGA raw data to reflectance units, is composed of several different steps outlined below. Global studies require processing large quantities of data, thus each step is constrained by the necessity of reducing the number of calculations to minimize data processing time. As a consequence, a few approximations are made and are described below.

3.1. Photometric Calibration

[10] OMEGA data are released as raw data cubes organized by the number of their acquisition orbit. These raw data cubes are composed by two spatial dimensions and one spectral dimension. An element of the spatial dimensions, a pixel, corresponds to an instantaneous field of view of 1.2 mrad and the spectral dimension is composed of 352 spectels (spectrum element). The spectel full width at half maximum (FWHM) is 20 nm for the L channel. Each spectel records the digitization of the light flux received by the detectors over its wavelength range as expressed in digital numbers. Each raw data cube is provided with a corresponding geometrical cube that gives information on the observations for each pixel (latitude and longitude coordinates, altimetry, solar incidence, etc.). There is a small spatial shift of one to three pixels between the C and L channels, depending on the number of the orbit, and a

shift correction has been applied on the basis of the geometry of the C channel data [Bibring *et al.*, 2004a].

[11] The flux received by the detectors comes from the Martian surface and atmosphere but also from the instrument itself. The OMEGA spectrometers are cooled to 190 K ; therefore no data emitted by the Martian surface for temperatures lower than 190 K can be obtained. The first step of data processing consists in subtracting the instrument radiation from every raw OMEGA spectrum. This radiation spectrum was measured during the transfer orbit by observing a dark sky area (about 20 ADU at $5 \mu\text{m}$). Digital numbers (DN) are then converted to physical units from which information about Mars can be deduced. For this purpose each raw spectrum is divided by the OMEGA transfer function and by the integration time of the observation (2.5 ms or 5 ms for C and L channels) to convert DN to radiance units. The energetic flux spectra received from the planet is expressed in $\text{Wm}^{-2}\mu\text{m}^{-1}\text{sr}^{-1}$. We model these light fluxes received by OMEGA as the summation of two components: the reflection of the solar light by the surface and the thermal emission of the surface, both being filtered by the atmosphere. We assume that surface reflection follows Lambert's law, such that

$$I = H_{\text{atm}}(\lambda) \cdot F_{\text{sum}} \cdot A(\lambda) \cdot \cos(i) + H'_{\text{atm}}(\lambda) \cdot \varepsilon(\lambda) \cdot B(T) \quad (1)$$

with

- I light intensity received by OMEGA;
- $H_{\text{atm}}(\lambda)$ atmospheric absorption for reflected part;
- $H'_{\text{atm}}(\lambda)$ atmospheric absorption for thermal part;
- $A(\lambda)$ albedo of the soil;
- F solar intensity received by the surface;
- i solar incidence (Lambert's law is assumed);
- $\varepsilon(\lambda)$ emissivity of the soil (supposed to be equal to $1-A(\lambda)$ according to Kirchhoff's law);
- B(T) emission of a blackbody at the temperature T.

[12] The goal of data processing is to retrieve the albedo spectrum, $A(\lambda)$, in order to compare it to library spectra and laboratory measurements. For the C channel, the observed radiance is dominated by the reflected component and the thermal contribution is insignificant for Mars surface temperatures. Examples of resulting $I/F\cos(i)$ spectra are presented in Figure 1. These spectra are clearly affected by atmospheric absorption, for example they are close to zero at $2.7 \mu\text{m}$ and $4.3 \mu\text{m}$ due to atmospheric CO_2 absorptions. This atmospheric contribution corresponds to the terms H_{atm} and H'_{atm} of equation (1) and has to be removed to retrieve the albedo spectrum. The most accurate method would consist in modeling the atmosphere and its effects on the light path before and after interacting with the surface for each observation time and location. Such a method is impractical because it requires a complete Martian atmospheric model with accurate knowledge of the temperature, pressure, dust and water ice opacity with a high spatial and temporal resolution [Melchiorri *et al.*, 2006] and would

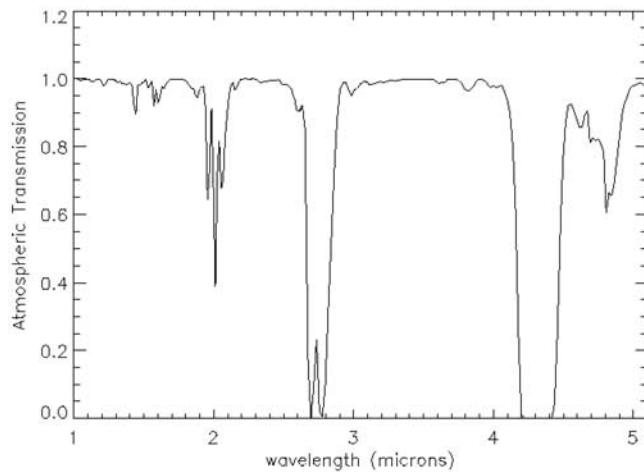


Figure 2. Transmission of the Martian atmosphere. This spectrum is calculated for a standard atmosphere using a radiative transfer model and is used to correct the atmospheric absorption on OMEGA spectra.

require a prohibitive calculation time. Therefore atmospheric contribution is extracted directly from OMEGA spectra and then removed by using the method described by *Langevin et al.* [2005b] and *Mustard et al.* [2005]. This method estimates the atmosphere optical depth of a given $I/F\cos(i)$ spectrum by scaling a reference atmospheric spectrum to the observed depth of the $2\ \mu\text{m}$ atmospheric CO_2 absorption. The OMEGA spectrum is then divided by the scaled reference spectrum. Figure 2 shows this reference spectrum which has been calculated assuming standard atmospheric conditions (T. Fouchet, personal communication, 2004).

[13] An example of the broad hydration band at $3\ \mu\text{m}$ observed in OMEGA spectra is presented in Figure 1. Since surface daytime temperature ranges between 200 K and 300 K on Mars, this band can be significantly affected by the thermal contribution. Figure 1 shows a strong increase of $I/F\cos(i)$ (atmosphere-corrected) with a blackbody shape corresponding to the thermal contribution described in equation (1). The surface temperatures and thus the thermal contributions are different for each spectrum and therefore the $3\ \mu\text{m}$ band cannot be compared directly between spectra without removing this component. A method is presented below to assess and remove the thermal contribution.

3.2. Removal of the Thermal Contribution

[14] Thermal removal consists of two steps: first, the assessment of the surface temperature for each pixel, and then the calculation of albedo corrected for thermal emission.

3.2.1. Assessment of Temperature

[15] The temperature of the Martian surface is the result of the equilibrium between solar flux and radiative and conductive losses. The resulting Martian daytime temperatures (from 200 K to 300 K) are responsible for a thermal emission that is observed by OMEGA above the atmosphere (see Figure 1). Our assessment of the temperature of a pixel is therefore directly derived from OMEGA $I/F\cos(i)$ (atmosphere-corrected) spectra, keeping in mind that this thermal flux is cooled weakly by the atmosphere.

[16] The wavelength region near $5\ \mu\text{m}$ is the best to assess the surface temperature since the relative proportion of thermally emitted radiance to reflected radiance is high and atmospheric absorption is very low in this region (Figure 2). Having a priori knowledge of the reflectance at $5\ \mu\text{m}$ would make it possible to deduce the thermal contribution. *Erard and Calvin* [1997] published average reflectance spectra of bright and dark Martian soils for OMEGA wavelengths. These reflectance spectra, that we name here reference spectra, were retrieved from the ISM instrument results after correction for thermal contribution. We assume that each OMEGA spectrum can be approximated as a linear combination of these two reference spectra over the wavelength range $2.3\text{--}2.5\ \mu\text{m}$, where thermal emission contribution is null. This linear combination provides an approximate value of the surface reflectance at $5\ \mu\text{m}$. This value is then compared to the observed OMEGA spectrum to determine the thermal contribution. This comparison assumes that H_{atm} and H'_{atm} of equation (1) are the same, though they are actually different since the atmospheric optical path of thermal emitted radiation is at least half that of reflected solar radiation. However, this approximation is valid because the atmospheric transmission is close to 1 at $5\ \mu\text{m}$. Finally, a least squares solution is used to fit the estimated thermal radiance to a theoretical blackbody to derive the surface temperature for each pixel. Figure 3 illustrates the steps of this method for typical high- and low-albedo soils.

[17] Our method for thermal correction is based on two main approximations: the $5\ \mu\text{m}$ reflectance value estimated from reference spectra, and the same atmospheric correction for reflected and thermal parts at $5\ \mu\text{m}$. We have tested the robustness of these approximations on several orbits, exhibiting high- and low-albedo areas, for associated temperatures between 230 K and 270 K. First, we know from laboratory reflectance spectra library that for the minerals thought to be present on Mars, reflectance value at $5\ \mu\text{m}$ can vary between factors $1/2$ to 2 of the value of our reference reflectance spectra. Using a half lower reference reflectance value at $5\ \mu\text{m}$ decreases temperature estimates by at most 1 K, and using a twice greater reference reflectance value increases temperatures estimate by at most 3 K. Second, our method corrects atmospheric absorption for thermal part at a too high level; when we compare it to the estimate of temperature without atmospheric correction we obtain an uncertainty of ~ 1 K. The total uncertainty on the derived temperature is therefore ~ 4 K.

3.2.2. Comparison With a Numerical Model

[18] To check the order of magnitude of the derived temperature, results were compared to the numerical simulation of the Martian Global Circulation Model [*Lewis et al.*, 1999; *Forget et al.*, 1999] for several orbits. This model provides the Martian surface temperature for the requested latitude, longitude, hour of the observed points, and the solar longitude of Mars. The data can be retrieved from the Martian Climate Database (MCD) with a grid of 3.75° by 3.75° . The comparison between OMEGA and MCD results for one orbit is presented in Figure 4. The discrepancy between the two data sets is at most ~ 10 K for a surface temperature of ~ 260 K, which corresponds to a relative difference of 4%. The method based on OMEGA data

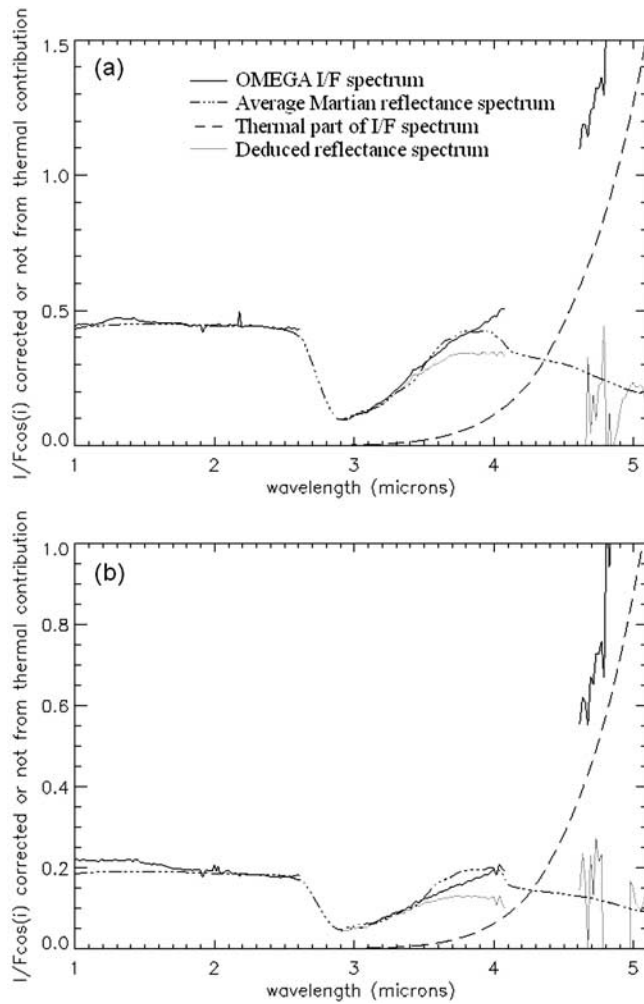


Figure 3. Illustration of the removal of thermal contribution (a) for a high-albedo point, $T = 273$ K, and (b) for a low-albedo point, $T = 252$ K, to get albedo spectrum. Data have been removed from 2.6 to 2.9 μm and from 4.15 to 4.6 μm because of strong atmospheric absorption (Figure 2). Black plain curve: $I/F\cos(i)$, without correction from thermal contribution (same spectra as the dotted curve in Figure 1). Dotted and dashed curve: average Martian albedo spectrum, used to assess thermal part at 5 μm . Dashed curve: derived estimation of thermal part divided by $F\cos(i)$. Gray plain curve: resulting albedo spectrum corrected from thermal contribution.

yields surface temperatures almost systematically below those of the numerical simulation. This difference is consistent with the fact that OMEGA observes the surface temperature above an aerosol-rich atmosphere, for which the effect of the dust is to reduce the radiance emitted by the surface by diffusion and absorption. The thermal emission of dust is constrained by its temperature, which is 40 K lower than the soil at 1 m above the surface at 2PM (local time) and 80 K lower at 1 km [Smith *et al.*, 2004].

3.2.3. Subtraction of Thermal Part

[19] Once the temperature of the OMEGA spectrum is known, the thermal contribution can be calculated for the whole wavelength range. Figure 3 presents the resulting thermal contribution curves associated with several pixels.

Equation (2), which is the inversion of equation (1), is used to retrieve the OMEGA reflectance spectrum from 2.9 μm to 5.1 μm . H'_{atm} is approximated by H_{atm} since atmospheric absorption is very low in the 2.9–4.0 μm range (Figure 2). Figure 3 presents the resulting reflectance curves for the full wavelength range (gray curve). The thermal correction is smooth from 2.9 μm to 4.1 μm . Conversely the correction is very rough beyond 4.6 μm because denominator is close to zero in equation (2) (reflected and thermal parts are equal), and because strong atmospheric absorption bands make the approximation H'_{atm} equal to H_{atm} inadequate in this wavelength range. OMEGA spectra are ready for assessment of the 3 μm band once the thermal contribution has been removed.

$$A = \frac{H_{\text{atm}}^{-1}(I) - B(T)}{F_{\text{sum}} \cdot \cos(i) - B(T)} \quad (2)$$

3.3. Data Selection

[20] Our analysis of the 3 μm region is restricted to a subset of the OMEGA data for several reasons. The first reason is that the response of the L channel varies with time. Comparison between data makes sense only if the observations are equally calibrated. Calibration spectra are available for each orbit and represent the response of the spectrometer to a calibration lamp. A survey of the calibration spectra for all orbits shows that the response of OMEGA to the calibration lamp is constant with time for the C channel. This proves that the calibration lamp has not varied with time. By contrast, the calibration spectra are not constant for the L channel. Figure 5a shows OMEGA response to calibration lamp in two extreme cases, a high (nominal) level and a low level. The effects of such calibration problems on albedo spectra can be seen in Figure 5b, where we present two observations of the same point, close in solar longitude, acquired approximately at the same hour, and with the same solar incidence. As expected, the C

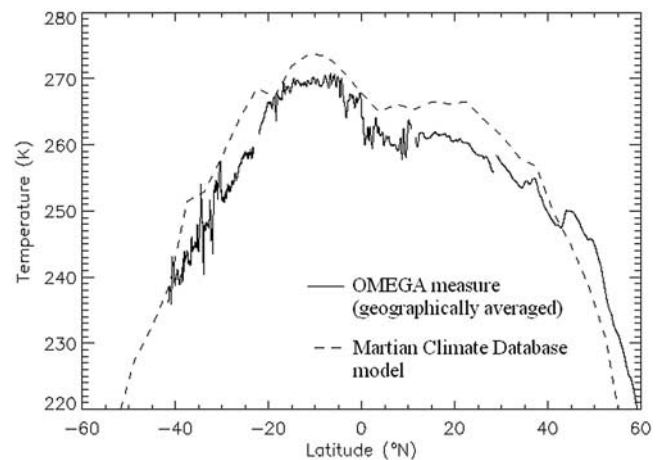


Figure 4. Comparison of the temperature above the atmosphere derived from OMEGA spectra at 5 μm (plain curve) with the surface temperature calculated by the Martian Climate Database (dashed curve) for the same latitude, longitude, hour, and date. Corresponding solar longitude is 11.2°.

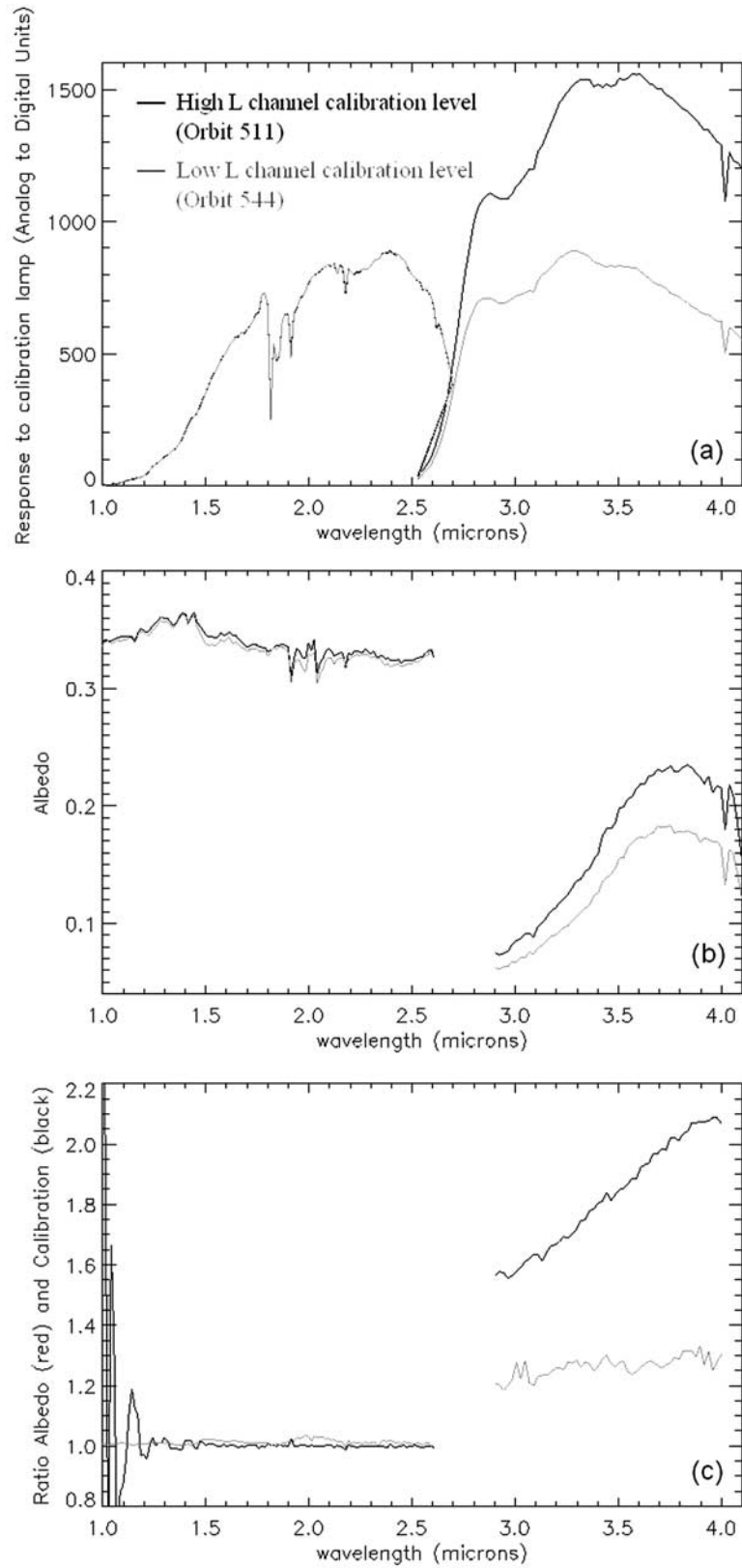


Figure 5

channel albedo spectra are the same, whereas those for the L channel are significantly different. The variations in albedo spectra are therefore strongly affected by the variations of the instrument response to the calibration lamp, and this influence is non-linear (Figure 5c). The origin of this phenomenon is still under investigation. In this paper, we deal only with observations for which the spectrometer is in the high state for the L channel, corresponding to orbits 31 to 502 and 923 to 1224. This represents 896 data cubes and corresponds to ~ 60 million spectra. We note that this calibration problem is also linked to the spatial shift between the C and L channels mentioned previously. This shift is about one pixel for observations corresponding to the high L channel calibration level and may increase to three pixels for the low L channel calibration level.

[21] During the nominal calibration state, we notice that for a few orbits the temperature of the detector at the time of the calibration response measurement may be warmer than is desirable for accurate data. This means that the calibration spectrum measurement was taken before the detector was completely cooled and is therefore not representative of the calibration state during the associated observations. We also notice that a few orbits are missing their associated calibration spectra. For these two situations where we do not have valid calibration measure, the associated observations were not excluded from global studies because they were acquired during nominal state of L channel, but they are not considered when we want to compare specific albedo spectra.

[22] A second reason why only a subset of the entire data set is analyzed is the presence of water ice on a large part of the OMEGA data set. Water ice may be present as frost deposited on the surface during winter or clouds in the atmosphere. It exhibits a strong absorption feature in the $3 \mu\text{m}$ range that hides the hydration absorption from minerals, therefore every OMEGA spectrum exhibiting water ice features must be ignored. Water ice can be detected by OMEGA through an absorption band at $1.5 \mu\text{m}$ [Gondet et al., 2006]. Every OMEGA spectrum exhibiting a $1.5 \mu\text{m}$ band depth stronger than 1% is therefore excluded from this analysis. We do not use a value of 0% for two reasons. First, OMEGA spectra have high signal-to-noise ratios in general (greater than 100), but noise may be responsible for band depths lower than 1%. Second, a slight non linearity of the detectors for the values of DN between ~ 800 and ~ 1700 at $1.5 \mu\text{m}$ may be responsible for variations in band strength of a few percents. This implies that some spectra unaffected by the presence of water ice, but which still exhibit a $1.5 \mu\text{m}$ band depth of 2–3% or less, were not processed.

[23] Furthermore, we do not consider OMEGA spectra acquired at emergence angles $>15^\circ$ and at solar incidence angles $>70^\circ$ from the normal vector, because the approximation of Lambertian emission becomes too rough. Ac-

counting for these exceptions, a total of ~ 35 million spectra have been processed to study the $3 \mu\text{m}$ absorption band. This provides a spatial coverage of one third of the Martian surface (for latitudes between 75°N and 75°S), with numerous overlapping tracks, enabling us to make temporal comparisons. Because of the acquisition epoch of the selected orbits and the elliptical orbit of Mars Express, the surface coverage is greater in the northern hemisphere than in the southern.

4. Hydration Quantitative Estimate

[24] The assessment of the $3 \mu\text{m}$ hydration feature is possible once reflectance spectra have been retrieved for the C and L channels. Several methods to measure the $3 \mu\text{m}$ absorption band strength from an albedo spectrum have been previously described in the literature. A recent study by Milliken and Mustard [2005] compares the accuracy of different band measurement methods for estimating absolute and relative water content for a variety of hydrated mineral compositions. Several of these methods are then applied by Milliken et al. [2007] to the OMEGA data set to estimate the absolute water content of the Martian surface. In this paper we consider two methods: the integrated band depth and the derivation of the water weight percentage through apparent absorbance.

4.1. Integrated Band Depth (IBD)

[25] A quantitative assessment of hydration is made by an integration of the band depth between a spectral continuum slope and the observed $3 \mu\text{m}$ band in each OMEGA spectrum. The relative band depths of every spectral between 2.9 to $3.7 \mu\text{m}$ are summed as exposed by equation (3).

$$IBD = \frac{1}{N} \sum_{\lambda_0=2.9\mu\text{m}}^{\lambda_w=3.7\mu\text{m}} \left(1 - \frac{\text{albedo}(\lambda)}{\text{continuum}(\lambda)} \right) \quad (3)$$

This method is similar to the *normalized IBD* used by Calvin [1997], except that, in our method, the continuum depends on the wavelength. Here, we use a linear continuum between $2.35 \mu\text{m}$ and $3.7 \mu\text{m}$, representing the general trend of the albedo spectrum in this area. OMEGA spectra at $2.35 \mu\text{m}$ and $3.7 \mu\text{m}$ are known to have a high signal-to-noise ratio and lack absorption features. In the integration the lower limit of $2.9 \mu\text{m}$ is selected because it corresponds to the end of the atmospheric CO_2 absorption band centered at $2.8 \mu\text{m}$. We point out that wavelengths longer than $3.8 \mu\text{m}$ are more affected by instrumental effects that are not described here. IBD is known to be albedo- and composition-dependent. The IBD also has the advantage of considering the $3 \mu\text{m}$ absorption as a broad band, accounting for its depth and its width.

Figure 5. Example of the influence of instrumental variations on reflectance spectra. (a) OMEGA responses to calibration lamp (C and L channels) for orbits 511 (black, high level) and 544 (gray, low level). (b) Two albedo spectra of the geographical point (321.5°E , 5°N), tracked twice at close times but with different calibration responses. Black: pixel from orbit 511 (high level). Gray: pixel from orbit 544 (low level). (c) Ratios of albedo spectra and of response to calibration lamp orbit 511/orbit 544. Black: ratio of calibration spectra of Figure 5a. Gray: ratio of corresponding albedos of Figure 5b. Variation in response to calibration lamp from high to low level implies variation on the measure of albedo spectra but not linear.

[26] The uncertainties on the absolute value of integrated band depth have two main origins. First, noise on OMEGA reflectance spectra is at most 1% of the signal for the majority of the data set. It induces a Gaussian noise of 0.16% on the value of IBD. The second uncertainty origin is due to the assessment of the temperature of an OMEGA spectrum: we saw in section 3.2.2 that the different approximations may cause an error of ~ 4 K. Such a temperature variation causes an IBD variation of 2% at most, the highest for dark spectra.

4.2. Absolute Water Weight Percentage (WP)

[27] We estimate the water content of the surface by comparing OMEGA reflectance spectra to laboratory measurements done by *Yen et al.* [1998]. In their works, near-infrared reflectance spectra are converted to apparent absorbance (negative natural logarithm of the reflectance) for several mixtures with various hydration states (2, 4, 6, and 8 wt.%): palagonite mixed with basalt, bentonite with basalt, gypsum with basalt and goethite with basalt. We choose to compare OMEGA data to a mixture of palagonite with basalt because the shape of this mixture is the most similar to the general shape of OMEGA reflectance spectra. Ratios between the apparent absorbance values at 3.0 μm and 3.7 μm of this mixture have been calculated for the four water contents. A function linking the value of the ratio to an amount of water mass percentage has been constructed assuming a linear interpolation between the different water contents (equation (4)). This linear assumption is valid for low water contents, whereas for higher water content the relationship is better represented by a power law [*Milliken and Mustard*, 2005]. OMEGA reflectance spectra are converted to apparent absorbance at 3 μm and 3.7 μm and the ratio between both is compared to this linear function. An estimate of the water mass percentage is then derived from this comparison. This second method has the advantage of giving an absolute estimate of the water content, but it is likely more albedo- and compositional-dependent since variations in grain size, albedo, and composition are not taken into account here. The width of the band, which could be linked to the form of water, is not assessed by this method.

$$WP = 8.93 * \frac{OMEGA_Albedo(3\mu m)}{OMEGA_Albedo(3.7\mu m)} - 3.01 \quad (4)$$

The uncertainty in the estimates of water weight percentage is ~ 2 wt.% according to the data of *Yen et al.* [1998]. This uncertainty is only valid for OMEGA data as long as the samples measured by *Yen et al.* [1998] are representative of the composition, albedo, and grain size of the Martian surface. When comparing these measurements to OMEGA reflectance spectra two uncertainties must be added: the OMEGA noise, which is less than 1%, and the temperature effect that changes the value at 3.7 μm . These effects result in an uncertainty of 10% at most.

5. Results and Interpretations

5.1. Overall Presence of the 3 μm Absorption Band

[28] The calculation of the integrated band depth and estimates of water percentage by mass has been performed

for the selected data set described in section 3.3. The OMEGA data extend a major result of ISM and IRS observations: the 3 μm hydration feature is observed everywhere on the Martian surface, regardless of albedo, elevation, latitude or composition. The depth of the 3 μm band varies from one region to another but the band never disappears in the data studied here. The IBD ranges between 0.25 and 0.52. The values derived for the water content range from 3 to 8 wt.% H_2O , sometimes up to 12 wt.% at latitudes higher than 60°N confirming previous results by *Poulet et al.* [2005b]. Estimates of the water content are roughly consistent with the analysis using other method presented in the companion paper [*Milliken et al.*, 2007].

[29] Several factors other than surface hydration could influence the 3 μm band observed by OMEGA. First *Calvin* [1997] noted that her normalized IBD was higher at extreme viewing geometries, suggesting that atmospheric dust had some “hydrated component”. The OMEGA data set provides spot pointing observation sequences which consist in observing approximately the same spot with strong variations of the emergence angle. Therefore only the amount of aerosols is modified during the acquisition. Such an observation over Hellas Basin (orbit 2668) has been analyzed. This reveals that the IBD decreases with increasing emergence angle (up to a factor $1/4$ for high emergence angles of 80° with regard to the outward normal to the reference ellipsoid.). This observation indicates that aerosols may be hydrated but in a less important manner than the surface. Since our data set excludes observations at too high solar incidences ($>70^\circ$) or emergences ($>15^\circ$), and since solar incidences of overlapping tracks never exceed 30°, we consider that the presence of aerosols in the atmosphere has a negligible influence on the 3 μm feature variability. This is consistent with the very well overlapping of the tracks acquired at different times by OMEGA (except in the latitudes 40°N–60°N; see section 5.5).

[30] Secondly, the presence of water ice patches on the surface, or water ice clouds in the atmosphere, could affect the 3 μm band we measure with OMEGA, since the spectral signature of water ice is dominated by a typical strong absorption band at 3 μm . We recall that water ice is also characterized by a strong 1.5 μm band that is used to remove spectra contaminated by water ice (section 3.3). However, the 3 μm absorption band of water ice is approximately twice as strong as the 1.5 μm feature. This implies that small patches of water ice at sub-pixel level could affect the 3 μm area without any detectable 1.5 μm feature. We performed linear combinations of a dust-like spectrum with water ice spectrum (grain size of 10 μm) at several amounts in order to detect the uncertainty of the water ice detection method on the IBD. The simulations reveal that a spatial proportion of 2.5% of water ice is necessary to get a 1.5 μm band depth greater than 2% (greater than the 0.5% exclusion threshold). This corresponds to an increase of ~ 0.02 of IBD at most, i.e., a contribution of $\sim 3\%$ to the IBD. Moreover the shape of the 3 μm band when little water ice is added to a surface spectrum is clearly different compared to surface hydration: water ice exhibits an absorption band close to saturation from 2.9 to 3.4 μm , whereas surface hydration is close to saturation from 2.9 to 3.1 μm . To conclude, spectra with very low proportion of water ice may remain after removing

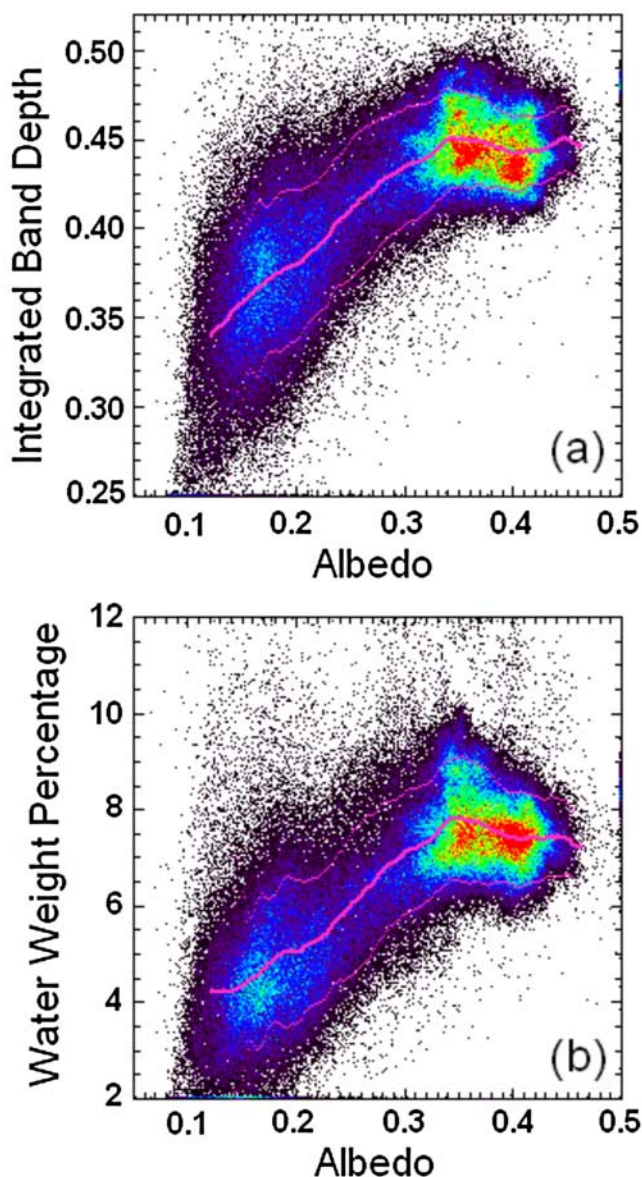


Figure 6. Evolution of hydration with albedo for the part of the OMEGA data set described in section 3.3. (a) The $3\ \mu\text{m}$ integrated band depth versus albedo. (b) Water mass content versus albedo. The data density is coded by a rainbow color scale, from black for a low amount of data to red for a large amount of data. The thick pink curve is the averaged IBD or WP of this distribution, and the two thin pink curves correspond to the 3 sigma variations.

all data with a detectable $1.5\ \mu\text{m}$ feature, but the quantitative effect on the $3\ \mu\text{m}$ band is negligible compared to surface hydration.

[31] Since the $3\ \mu\text{m}$ band is best explained by the hydration of the surface, the overall presence of the $3\ \mu\text{m}$ band regardless of surface composition supports the idea that the associated form of water is surface-adsorbed. This is indeed the only hydration form that can interact with every mineral. We emphasize that according to *Richard et al.* [2006], even if the relative humidity in contact with minerals is low (but not null), chemisorption exists and forms

metal-OH bonds at the surface of minerals. This phenomenon produces localized hydrophilic sites that fix water rather than other adsorptive gases such as carbon dioxide.

[32] Nevertheless, laboratory studies trying to estimate the water content of Martian-like samples tend to show that surface adsorbed water cannot easily explain the derived estimates of water content of a few percent at minimum. *Zent and Quinn* [1997] indeed showed that adsorbed water in minerals like basalts or clays could not exceed 1 wt.% in mass percentage under Mars P-T conditions. *Milliken and Mustard* [2005] or *Jänchen et al.* [2006] found higher values but tested only minerals with structurally adsorbed water (e.g., H_2O in clays, zeolites, sulfates). OMEGA was not able to detect such minerals on global scales on Mars. Moreover the water contents derived from OMEGA data are greater than those measured at the Viking Lander 1, 2 and Pathfinder sites. These landers measured water contents of the order of 1–2 wt% [*Foley et al.*, 2003; *Biemann et al.*, 1977; *Anderson and Tice*, 1979]. Though the instruments on these landers had large uncertainties because they were not designed to measure water content, the difference between the measurements of the landers and the values derived from OMEGA data could be significant.

[33] Recent results from the Mars Exploration Rovers confirm that an alteration layer may be present on the top surface of all rocks over the entire planet. More precisely, the uppermost millimeters of the Martian surface are composed of alteration products [*Hurowitz et al.*, 2006]. This coating may result from alteration occurring ~ 3 Ga ago of rocks in a global acidic environment with low water to rock ratios. On the other hand, *Yen et al.* [2005] explained the MER measurements of Bromine concentrations by a chemical alteration due to the contact of few layers of adsorbed water over geologic timescales under climatic conditions similar to present-day. In any case, this altered layer should likely exhibit the presence of hydroxyl groups or bound water, which could enhance the $3\ \mu\text{m}$ hydration band. The largest contribution of water content as seen by OMEGA could therefore come from either the surface-adsorbed water in the dust layer or from this alteration layer.

5.2. Albedo Dependence

[34] Only the regions at latitudes between 50°N and 50°S have been considered in this study because the high latitudes ($>50^\circ$) reveal large and unusual hydration features [*Poulet et al.*, 2005b; *Milliken et al.*, 2007]. Figure 6 shows the value of the $3\ \mu\text{m}$ IBD and estimated water content versus the albedo. A color scale is applied to show the relative density of the amount of data. This illustrates that the bright soils (albedo values from 0.3 to 0.45) are better represented than the darker ones. A general increase with a logarithm-like shape of hydration versus albedo is observed. This albedo dependence does not exist for the albedos larger than 35%.

[35] This albedo dependence is certainly partly explained by the method of measurement. *Milliken and Mustard* [2005] showed that the IBD was correlated to albedo when derived from reflectance spectra. For instance, adding black carbon to laboratory samples changes the IBD value without modifying the water content. Another method for estimating water content from OMEGA data does not detect this trend [*Milliken et al.*, 2007]. However, it assumes different strong

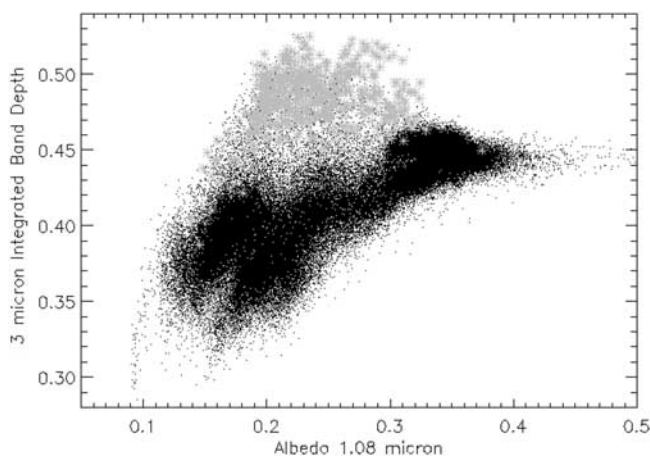


Figure 7. Correlation between IBD and albedo for all points of an OMEGA data cube exhibiting Mawrth Vallis. Black points correspond to pixels of the cube where the $1.9 \mu\text{m}$ hydration band is low or null (under 3% band depth); gray crosses correspond to pixels of the cube where the $1.9 \mu\text{m}$ band is enhanced (greater than 3%). Black points are organized on a general trend corresponding to the albedo dependence of IBD described in section 5.2.

hypotheses such as converting reflectance to single scattering albedo using Hapke modeling [Hapke, 1993], same composition and similar particle size ranges for bright and dark regions, although the surface of Mars is known to have different mineral compositions and different particle sizes. Specifically, brighter regions are dominated spectrally by ferric nanophase oxides, whereas the low-albedo terrains are modeled best by basaltic compositions with grain sizes of a few tens to hundreds of micrometers [Poulet *et al.*, 2007]. Therefore the dependence of hydration with albedo must have partly a physical origin: variations of composition and particle size, which affect the albedo, must be responsible for the variations of water content as well. For instance, smaller particles imply a higher surface to volume ratio, so potentially higher capacity of water adsorption [Zent and Quinn, 1997]. Moreover, the difference in oxidation state between low-albedo and bright regions as seen by OMEGA likely results from weathering processes [Poulet *et al.*, 2007], increasing the possibility to have structural water in the bright regolith. This interpretation is consistent with the detection by MGS/TES of an H_2O -bearing mineral in the Martian surface dust [Ruff, 2004].

[36] A physical process could also play an important role in the difference of hydration between dark and bright regions: darker soils absorb more light and are hotter. The adsorption isotherms of Zent and Quinn [1997] or the adsorption isobars of Jänchen *et al.* [2006], show a decreasing amount of adsorbed water with an increasing temperature. Dark soils are thus expected to be less hydrated.

[37] Plotting the estimated water weight percentage versus albedo (Figure 6b) shows the same trend with albedo as the IBD parameter, where both increase with albedo. We derive water contents of ~ 3 wt.% for dark soils (albedo about 0.2) and ~ 8 wt.% for bright soils (albedo of ~ 0.4). Again, these estimates are model dependent and do not account for the effects of varying composition and particle size on the

strength of the $3 \mu\text{m}$ band. Lower values for the bright units have been derived by Milliken *et al.* [2007].

[38] In conclusion the IBD-albedo dependence is likely caused by real variations of the hydration of the soils, while a part of the dependence may result from the measurement method. The quantitative contribution of each effect is still open because our knowledge of the surface of Mars (composition, grain size) is not constrained enough at the microscopic level. Every comparison of albedo spectra made in this study will therefore be done only when the continuum spectra are at a same level.

5.3. Correlation With the $1.9 \mu\text{m}$ Band

[39] Hydrated minerals such as phyllosilicates and sulfates have been detected by OMEGA on the Martian surface, mainly through the detection of the combination overtone $1.9 \mu\text{m}$ hydration band [Poulet *et al.*, 2005a; Arvidson *et al.*, 2005; Gendrin *et al.*, 2005]. Here we examine the relationship between the 1.9 and $3 \mu\text{m}$ bands for two regions: Mawrth Vallis for phyllosilicate-rich deposits, and Terra Meridiani for sulfate-rich terrains.

[40] Figure 7 shows the correlation between IBD and albedo over Mawrth Vallis (orbit 353). The main sequence, in black, shows the IBD albedo dependence described in the previous section. The points of the OMEGA cube exhibiting an enhanced $1.9 \mu\text{m}$ band, corresponding to clays (in gray crosses), have a significantly stronger hydration band at $3 \mu\text{m}$ than what is observed for other points corresponding to similar albedo values. This suggests that this hydration enhancement is not correlated to albedo. Figure 8 compares albedo, the $1.9 \mu\text{m}$ absorption band depth, the $3 \mu\text{m}$ IBD, and the water content derived for orbit 353. Clays are detected in places where the $1.9 \mu\text{m}$ band is enhanced, mainly on outcrops of the valley sides. The IBD at $3 \mu\text{m}$ is clearly greater in places where clays are present and exhibits an excellent spatial correlation. The IBD values for these outcrops are greater than the main data trend and vary from 0.45 to 0.52. Phyllosilicates therefore have an enhanced absorption at $3 \mu\text{m}$. The associated water percentages range between 7 wt.% and 9 wt.%, whereas terrains of similar albedo but without phyllosilicates have a percentage of around 5 wt.%. Other methods of estimating water content, as presented in the companion paper, indicate similar water contents.

[41] Figure 9 presents a map of OMEGA data (albedo, $1.93 \mu\text{m}$ feature and $3 \mu\text{m}$ IBD) over Terra Meridiani, where the $1.9 \mu\text{m}$ band has been detected [Gendrin *et al.*, 2005]. Unlike Mawrth Vallis, the $1.9 \mu\text{m}$ band in this region is due to the presence of sulfates and hydroxides. The $3 \mu\text{m}$ IBD is enhanced where the $1.9 \mu\text{m}$ band is detected, with associated water percentages between 7 wt.% and 8 wt.% (estimated as 5 to 7 wt.% in the companion paper), corresponding to an increase of 1–3 wt.% H_2O relative to surrounding areas. We notice that the terrains where the $3 \mu\text{m}$ IBD is enhanced cover larger areas than the terrains with a $1.9 \mu\text{m}$ band depth, and the corresponding peak concentrations are shifted. This can be explained by the fact that different forms of hydration influence the 1.9 and $3 \mu\text{m}$ bands. Actually, the $3 \mu\text{m}$ IBD map shows increased hydration over the entire etched terrains unit [Arvidson *et al.*, 2005], reinforcing the potential evidence of formation of this unit by fluid flow and/or precipitation. The zone 1

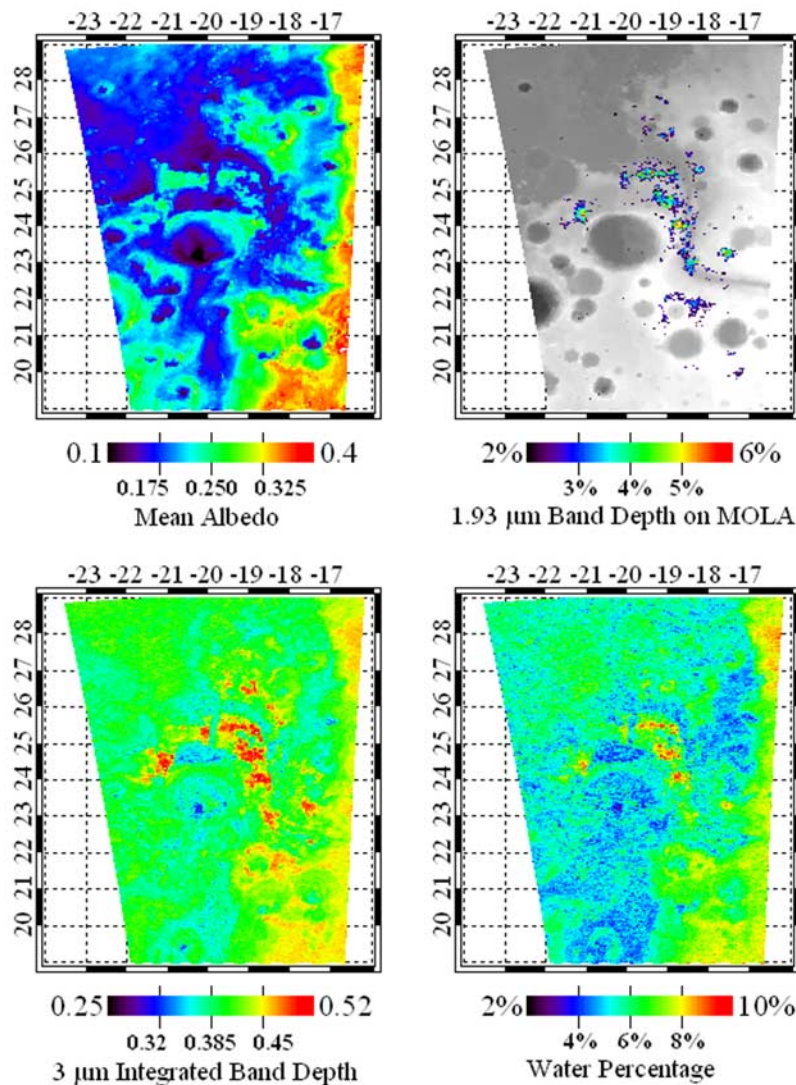


Figure 8. Albedo map, 1.93 μm band depth over altimetry MOLA map, integrated band depth map, and water percentage map over Mawrth Vallis. Data from third cube of orbit 353 are projected on a Martian planisphere with a resolution of 32 pixels/degree. The 1.93 μm absorption band is located in places where clays are present.

(Figure 9), where previous studies have detected monohydrated sulfates [Arvidson *et al.*, 2005], reveals that this area also exhibits a decrease in the strength of the 3 μm band, demonstrating that methods based solely on the 3 μm band are very sensitive to slight changes in water content.

[42] These two examples show that the 3 μm band is influenced by changes in composition and may provide additional information on the state of minerals and their water content. The enhancement of the 3 μm band for clay- and sulfate-rich regions is best explained by the direct influence of additional structurally adsorbed water on the band strength. In order to determine if the shape of the 3 μm band can be used to determine additional information regarding composition, Figure 10a presents the ratios of two reflectance spectra, one from the phyllosilicate-rich regions and one from outside this region but at a similar continuum level. There is no particular difference in the shape of the 3 μm absorption band when the composition

changes, except for an enhancement of the depth of the band for every wavelength between 2.9 μm and 3.8 μm . Figure 10b illustrates the same exercise for sulfate regions. The 3 μm band is deeper and wider for the sulfate-rich rock. We conclude therefore that composition can influence the shape of the hydration band, possibly because the form of water and the energy levels at which it is held are different. This observed composition dependence of the 3 μm band is consistent with our previous interpretation that the trend of IBD with albedo has also a physical origin.

5.4. Correlation With the Elevation of Ground

[43] Zent and Quinn [1997] and Jänchen *et al.* [2006] published isotherms to describe the adsorption of water on Mars soils. These isotherms show a dependence of the amount of adsorbed water with the partial pressure of water vapor. As Mars surface altitudes vary in a range of about 30 km, the atmospheric pressure applying on rocks and so the water partial pressure are significantly lower for regions

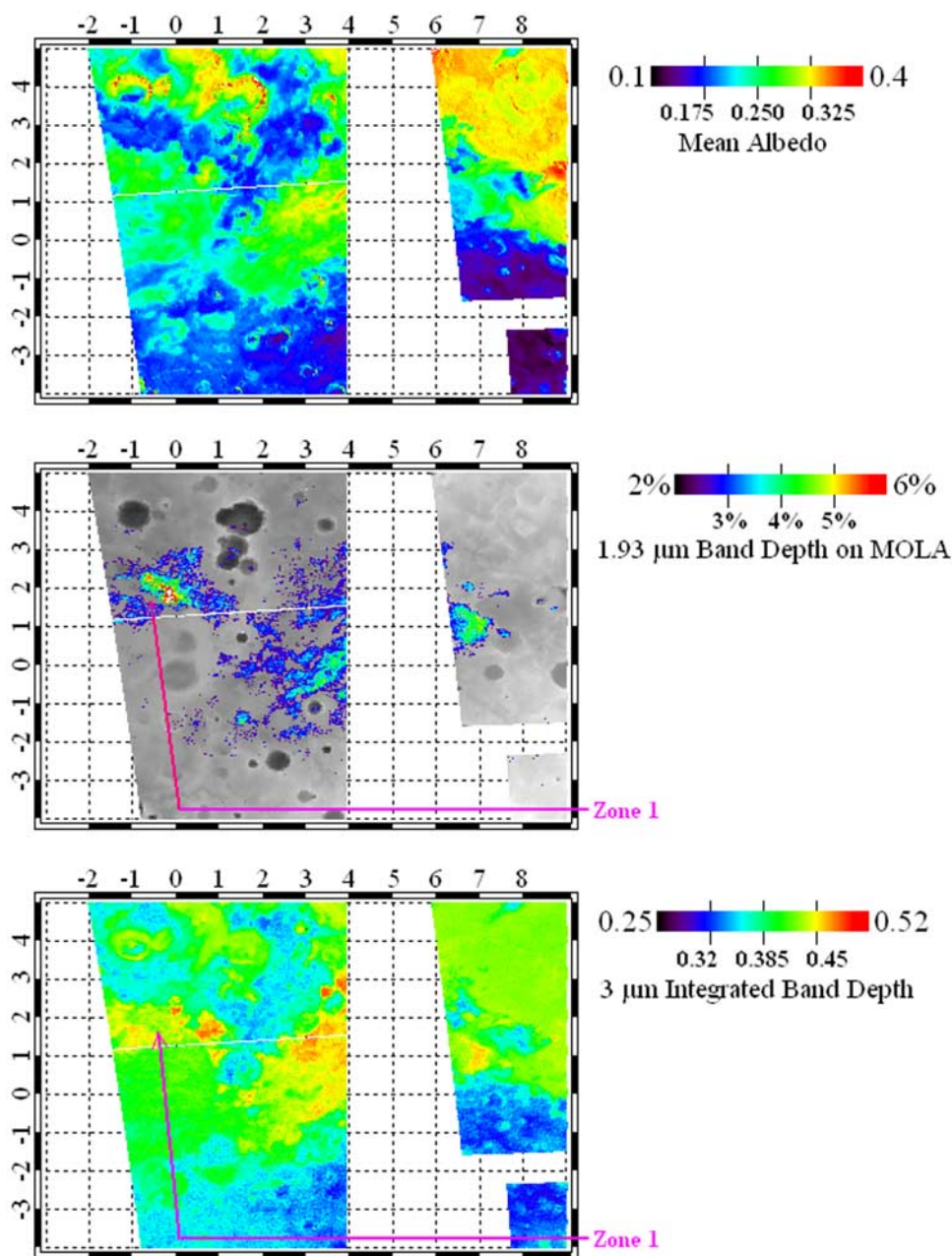


Figure 9. Albedo map, $1.93\ \mu\text{m}$ band depth over altimetry MOLA map, and integrated band depth map over Terra Meridiani (orbits 430 and 485). Data are projected on a Martian planisphere with a resolution of 32 pixels/degree. The $1.93\ \mu\text{m}$ absorption band is located in places where sulfates and hydroxides are present. The area shown by arrows is the zone where monohydrated sulfates have been identified [Arvidson *et al.*, 2005].

of high altitudes. The amount of adsorbed water would be therefore lower for higher altitudes. If the $3\ \mu\text{m}$ hydration band is largely due to adsorbed water, it should therefore exhibit this altitude dependence.

[44] Figure 11a shows the integrated band depth versus the MOLA altimetry for the data set selected above between 50°N and 50°S . The IBD values are classified by ranges of albedo (0.15 to 0.40 with an interval of 0.05) for which only the average IBD value versus altimetry is plotted. Classifying in albedo ranges avoids interference between albedo dependence effect and altimetry dependence effect. The

linear regression weighted by the data density is plotted for each class of albedo (dashed lines). For albedo between 0.15 and 0.35 the regression exhibits a small decrease of hydration with altitude. This trend is in agreement with the prediction from the adsorption isotherms. Figure 11b shows that the data set used here is not equally distributed, there is much more data in the northern hemisphere which is at lower altitude and which was observed just after winter when temporary frost may influence the amount of water (see section 5.5). This trend with elevation will have therefore to be checked when the entire OMEGA L channel

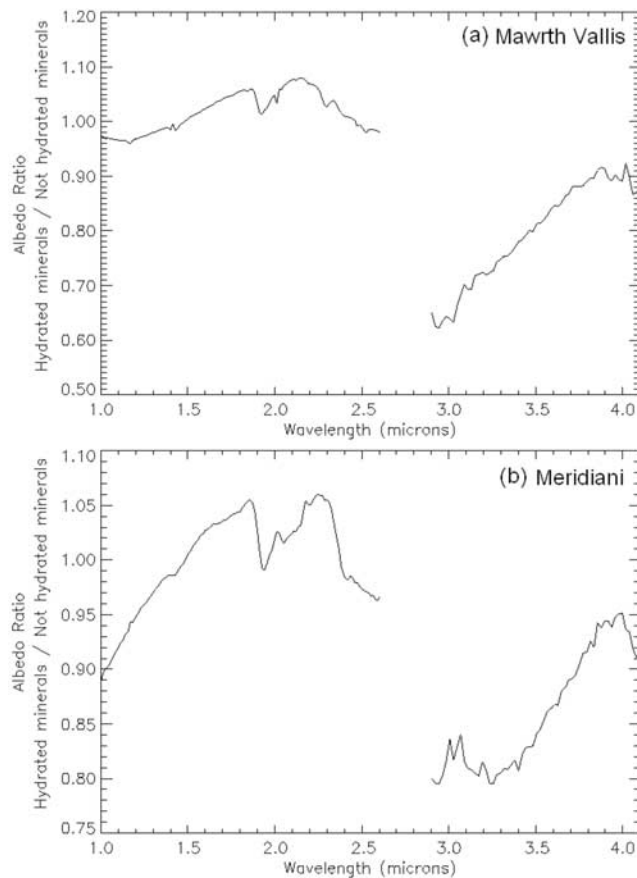


Figure 10. Ratio between the reflectance spectra of a hydrated-mineral region and a hydrated-mineral-free region of the same albedo. (a) Hydrated mineral is phyllosilicates. (b) Hydrated mineral is sulfates.

data is usable. In particular there is still uncertainty on the trend slopes. This likely variation of the amount of adsorbed water with elevation implies important consequences for the alteration processes. *Yen et al.* [2005] suggest that adsorbed water plays a role in the current alteration of minerals; in such a case, the lower altitude regions would be more easily altered by the present atmospheric conditions.

[45] Figure 11c shows that brightest soils (albedo around 0.4) do not exhibit this decrease of hydration with the elevation of ground. Data about bright soils present a wide altimetry range thanks to the high altitude of the Tharsis region. As bright soils are known to be mostly composed of dust, we could explain this lack of correlation between hydration and elevation by the constant renewal of dust all over the planet, due to aeolian transport. If so, the hydration variations due to elevation have to be slower than the distribution process. Dust is therefore exposed to an average water vapor partial pressure.

5.5. Seasonal Variations of Hydration

5.5.1. Detections

[46] For most places of Mars, the hydration measurements of overlapping orbits are the same. However, most of the regions located 40°N to 60°N do not show the same content of hydration at two different times, suggesting a

temporal evolution. This difference of overlapping tracks is illustrated by an example on Figure 12. On this region a green track (2004 summer observation, less hydrated) overlaps a mostly yellow and red track (2004 spring observation, more hydrated). Note that the associated solar longitudes are approximately 30° and 100°, corresponding to spring and summer, respectively, in the northern hemisphere.

[47] Two examples among several where the 3 μm band depth has changed in time are presented in Figure 13. The spectrum taken at the beginning of spring (black curve, May and April 2004, respectively) exhibits a deeper 3 μm band than the one taken at the beginning of summer (red curve, both October 2004). At 3.0 μm the relative difference of the albedo spectra inside the band is about 15%, whereas there is nearly no difference in the rest of the spectra. The associated IBD exhibit a variation of about 10%, and the associated water contents a variation of a couple of weight percent (1.75 and 1.45 wt.%, respectively).

[48] We will now discuss the different possible origins of these variations. For each example, the calibration responses of the spring and summer spectra are the same, and the temperatures of the calibration lamp at the times of the response measure are nominal. These temperatures stay at nominal level during all observation. In section 4.1 uncertainties about IBD due to noise and temperature assessment are about 2%, thus it is lower than the temporal variation. This implies that the temporal evolution does not result from an instrumental or method effect. We also checked whether the evolution could be due to an atmospheric effect. The presence of aerosols usually makes the continuum of the albedo spectrum bluer in the NIR and modifies average level. The constant shape of the C channel between black and red curves on Figure 13 is consistent with a constant amount of dust in the atmosphere. Actually, TES measurements confirm that dust opacity from 1999 to 2004 is constant between spring and summer for the locations of Figure 13 [Smith, 2006]. Moreover, we evaluated in section 5.1 that the quantitative effect of aerosols on the 3 μm band is very likely to be negligible. The temporal evolution is therefore not due to aerosols in the atmosphere. Moreover, the only difference in the C channels on Figure 13 occurs at 2.6 μm , with the apparition of an absorption band from spring to summer attributed to water vapor [Encrenaz et al., 2005]. This is consistent with TES observations indicating that the water vapor column increases between the two observations [Smith, 2006]. This increase of water vapor actually has a reverse trend compared to the 3 μm band and is therefore not responsible for the variation of the 3 μm hydration band. Last, the lack of any other absorption feature from spring to summer supports that there is no variation in surface composition, for instance ice deposition/sublimation or dust deposition/removal. As a consequence we can conclude that the 3 μm feature variation is due to the variation of the amount of water associated with the minerals.

[49] The hydration enrichment observed at the beginning of spring on Figure 13 has also been studied from a spatial distribution point of view. An example of the values of the albedo and hydration is shown on Figure 14. These data were acquired at the beginning of spring when solar

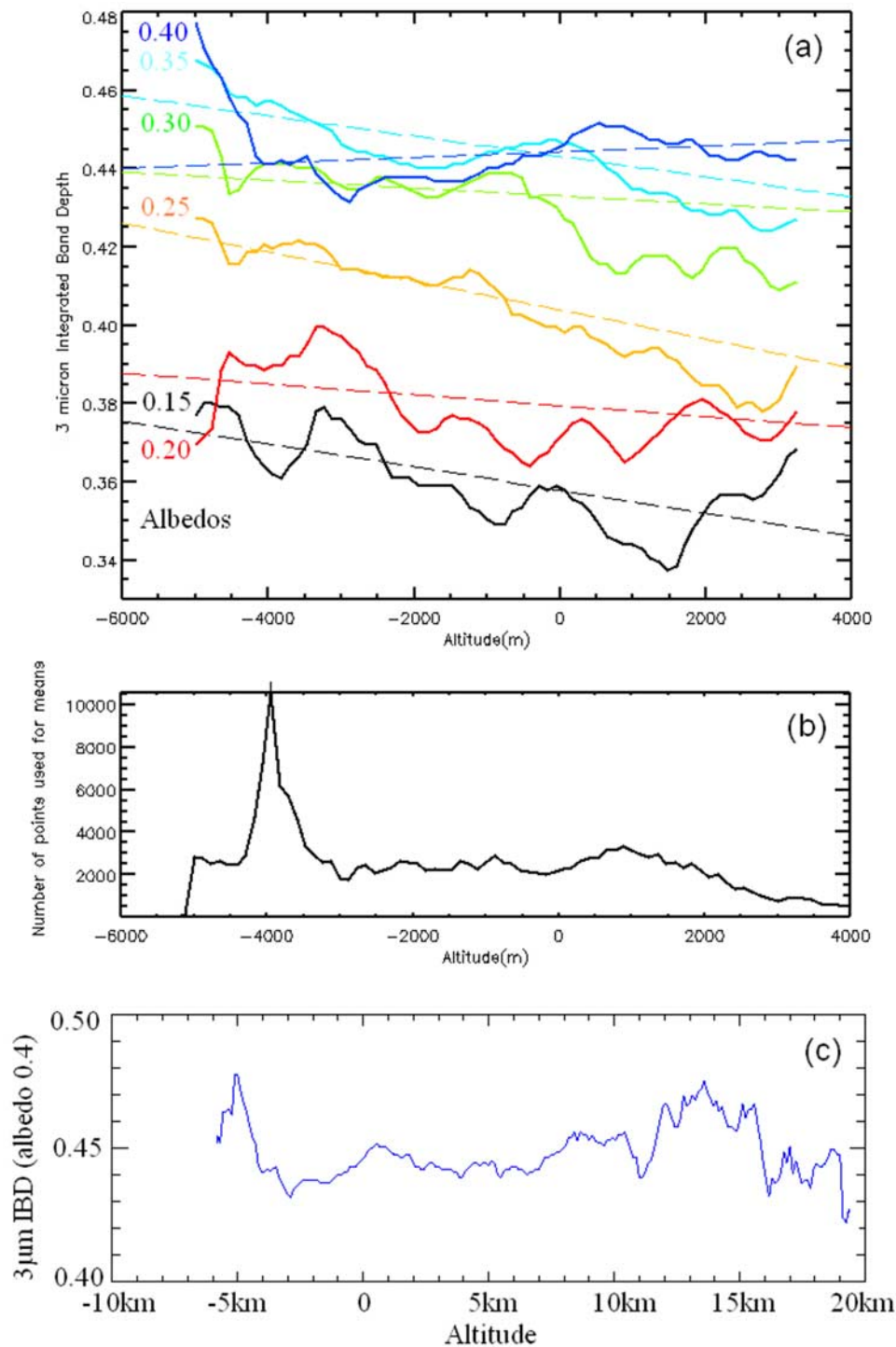


Figure 11. Evolution of hydration with elevation. (a) Average of the 3 μm integrated band depth versus elevation for albedo ranges: [0.125, 0.175], [0.175, 0.225], [0.225, 0.275], [0.275, 0.325], [0.325, 0.375], and [0.375, 0.425]. The dashed lines correspond to the linear regression of each curve weighted by the number of data (shown in Figure 11b). (b) Density of processed data for each altitude. (c) Average of the 3 μm integrated band depth versus elevation for albedo range [0.375, 0.425] for a larger range of altitude (-10 km to 20 km). The data at highest altitudes are observed on the Tharsis region.

longitude was 26.5° . We notice that for latitudes greater than 30°N , hydration is not spatially uniform but it increases with latitude. This is not an albedo effect since albedo is constant for the corresponding region. This trend is also observed for other orbits observed at similar times.

5.5.2. Dehydration Phenomenon

[50] Considering the periods and locations of the observations, the temporal evolution seems to be seasonal and due to the influence of water frost during winter. VL2 [see, e.g., *Svitek and Murray, 1990*], located at 48.67°N ,

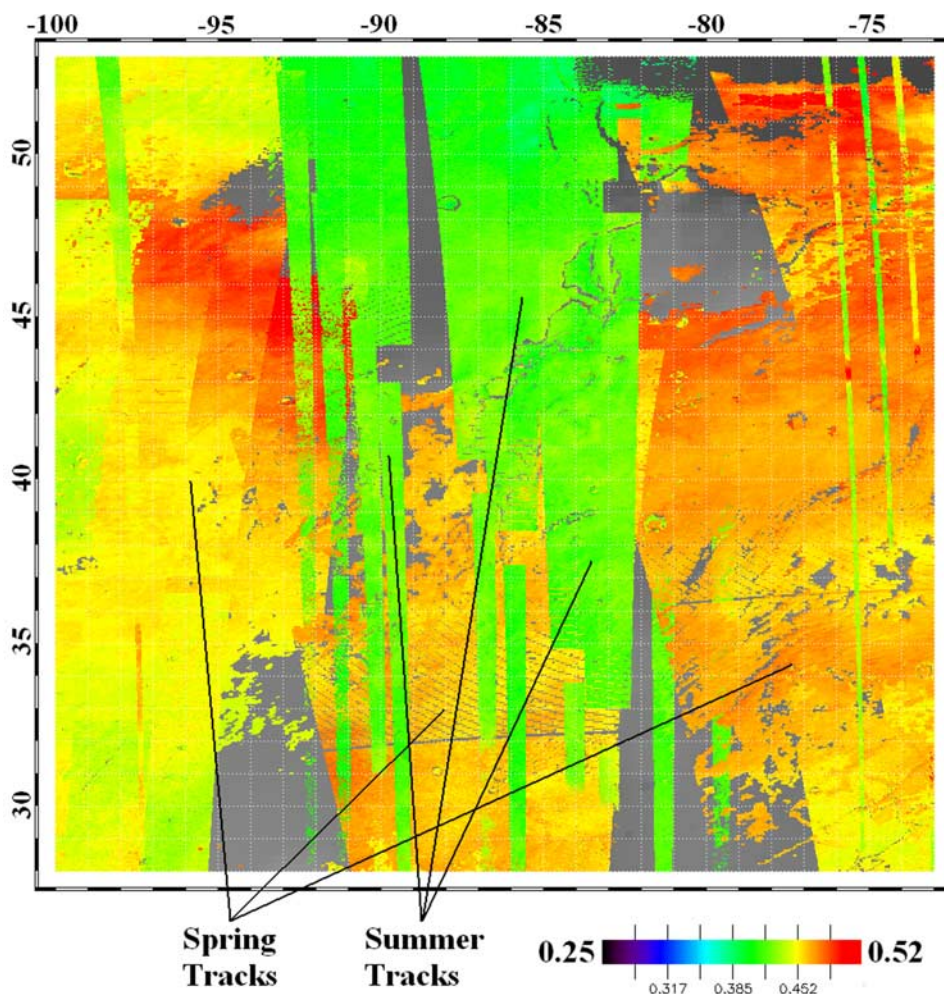


Figure 12. Example of a region (-95°E to -75°E , 30°N to 50°N) where summer tracks, less hydrated (in green), overlap spring tracks, more hydrated (in yellow and orange). Gray areas: no data.

134.01°E , observed the presence of water frost during winter as a thin layer. OMEGA confirmed this presence [Schmitt *et al.*, 2005] for large part of latitudes 40°N – 60°N . The presence of water frost during a long period (at least eight months in autumn and winter) probably enriches the hydration of minerals. At the end of winter, sun makes frost sublimate leading to highly hydrated minerals at the beginning of spring (Figure 13). During all spring and during the beginning of summer, the hydration of surface minerals goes back to equilibrium with water partial pressure of the atmosphere. At the beginning of summer a lower hydration of the soil is detected. The hydration enrichment with latitude, observed on Figure 14, is consistent with this interpretation: the amount of frost deposited on the surface during winter increases with latitude up to the pole. The more water ice is in contact with minerals in winter, the more water the minerals hold at the end of winter.

[51] The soil temperature at the times of observation is also likely to play a role in these hydration amounts. Jänchen *et al.* [2006] or Zent and Quinn [1997] published isotherms and isobars of adsorption for several minerals. The curves at water vapor partial pressure of 0.001 mbar

show clearly that the adsorption capacity of minerals decreases with temperature and this decrease is of the order of water weight percents for the Martian temperatures. The average diurnal temperature at the solar longitudes of observations on Figure 16a are 203 K for $\text{Ls} = 30^{\circ}$ and 213 K for $\text{Ls} = 100^{\circ}$ (from Martian Climate Database [Lewis *et al.*, 1999]). This discrepancy applied to the isobars of Jänchen *et al.* [2006] gives water content variations of a few wt.% in agreement with our observations. The reduction of adsorption capacity due to temperature, and the presence of frost in winter as a source for water molecules, can explain these seasonal hydration variations.

[52] It is possible to object that the hydration variations observed by OMEGA could also be due to diurnal variations. Indeed the diurnal range of temperatures may reach 100 K and confronted to isobars of Jänchen *et al.* [2006], this implies large hydration variations. Numerical simulations [Böttger *et al.*, 2005] show an increase of water content in the regolith during nighttime because of a lower temperature. On Figure 13a, the spring and summer observations were acquired at 10.30 and 16.00 (local time), respectively, for OMEGA surface temperatures corresponding

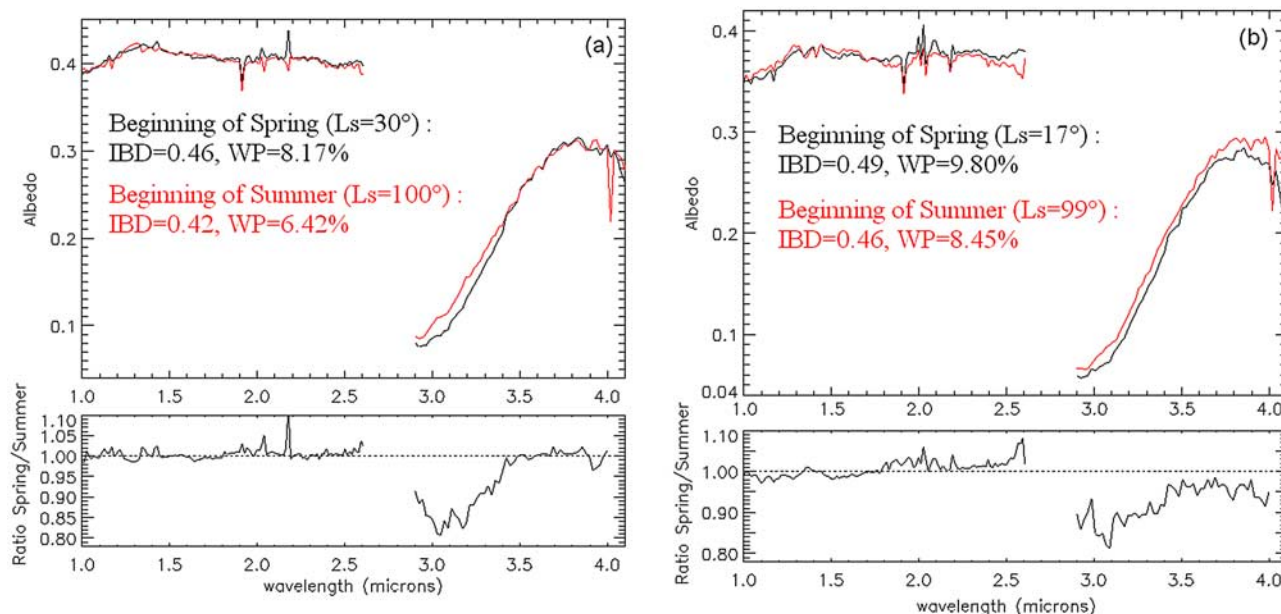


Figure 13. Example of seasonal variations: comparison of the reflectance spectra for two points between the beginning of spring and the beginning of summer. Temperatures of the detector at the times of measurement are nominal and equal to -196°C . (a) Albedo spectra of the observed point (-84°E , 41°N) visible on Figure 12 at $L_s = 30^{\circ}$ (black curve, beginning of spring) and $L_s = 100^{\circ}$ (red curve, beginning of summer). Integrated band depth varies from 0.465 to 0.431; water percentage varies from 8.64 wt.% to 6.95 wt.%. The associated water content evolutions of the companion paper are approximately 2 wt.%. (b) Albedo spectra of the observed point (-148°E , 47°N) at $L_s = 16.9^{\circ}$ (black curve, beginning of spring) and $L_s = 98.6^{\circ}$ (red curve). IBD varies from 0.489 to 0.461; WP varies from 9.76% to 8.29%.

to 260 K and 251 K, respectively. The temperature variation is therefore small and opposite to the hydration evolution. Moreover the kinetics of adsorption is a quite slow phenomenon, for instance *Jänchen et al.* [2006] need a couple of days to reach equilibrium. These two arguments lead us to think that the diurnal variation should not involve large amounts of water, compared to seasonal variations.

[53] The kinetics of this dehydration phenomenon occurring from the end of winter to the beginning of summer could be studied through the comparison of hydration on such soils at different times in spring. Unfortunately we do not have enough data to perform such a survey. In particular the end of dehydration kinetics cannot be studied because of the lack of data from orbit 500 to orbit 900. Nevertheless, some observations give some useful indication on how this dehydration phenomenon evolved in time. The albedo spectra of the point 48°N , -102°E for solar longitudes of 20° and 27° are shown on Figure 15. The temporal shift is low, equal to 13.4 sols, but the dehydration phenomenon is significant, with an IBD going from 0.46 to 0.44. As for Figure 13 the different instrumental and physical processes have been checked to prove that this phenomenon is due to the surface hydration. The decrease of IBD, in a solar longitude variation of 7° , is already half the one for solar longitude variation of 70° . This point requires confirmation by further observations, but the dehydration seems to be maxima at the beginning of spring, when frost has just sublimated and rocks are insulated by sun. It confirms kinetics proportional to the amount of adsorbed water.

[54] Figure 16 shows another region where the dehydration phenomenon is observed. It plots the hydration value versus latitude for two overlapping orbits at the beginning of spring ($L_s = 18^{\circ}$) and summer ($L_s = 115^{\circ}$). The hydration increase with latitude in spring is very clear on this figure, while the dependence with latitude has disappeared. Moreover we can see that the whole summer track has approximately the same hydration rate than the bottom spring track (corresponding to lowest latitudes, under 40°N). This confirms that soils under 40°N are not concerned by the wintry hydration enrichment, since the IBD is the same in spring and in summer. No water ice is deposited in winter. This also shows that the soil beyond 40°N has come back into balance with the atmosphere in summer.

5.5.3. Discussion

[55] Two arguments lead us to think that the form of water associated with these seasonal variations of hydration must be in major part surface-adsorbed water. First, these seasonal variations imply a very exchangeable form of water, and surface-adsorption requires the lowest energy levels. Second, the spring hydration decrease is observed between 40°N and 60°N on the whole planet, whatever the albedo, the composition or the altitude is. Surface-adsorbed water is the only hydration form that can interact with every kind of mineral, reinforcing the idea that this form of hydration is likely to be responsible for the temporal variation. Finally, if we compare the dehydration kinetics as seen by OMEGA on Figure 13 and Figure 15 to the dehydration laboratory measurements in dry air [*Milliken and Mustard*, 2005], we can notice that the laboratory

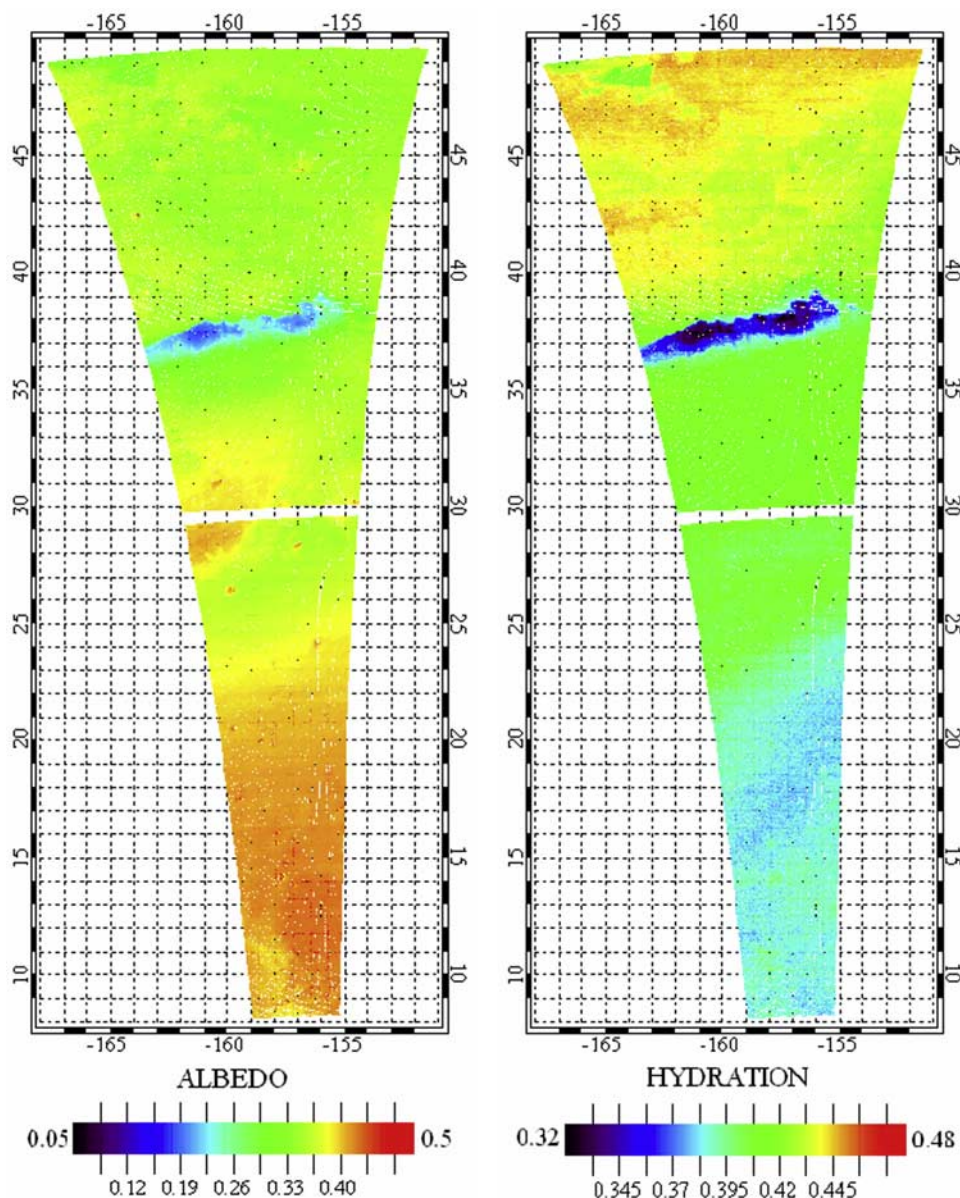


Figure 14. Albedo at $1.04 \mu\text{m}$ and IBD criteria with color scale of data cubes 351_3, 4, and 5 ($L_s = 26.5^\circ$, beginning of spring). From 25°N , albedo is constant with latitude, whereas hydration at $3 \mu\text{m}$ increases.

desorption spectral shapes are very similar to the evolution of the OMEGA dehydration spectra. This suggests that similar phenomena of desorption occur.

[56] The water content variation observed with our method and also with the method of the companion paper is about 2–3 wt.%. This result is consistent with the isobars of *Jänchen et al.* [2006] but not with the isotherms of *Zent and Quinn* [1997]. If our water content measurement methods are too high and if the Martian soil is better modeled by the isotherms of *Zent and Quinn* [1997], then surface-adsorbed water cannot be sufficient to explain these seasonal variations. This would suggest that other hydration forms, such as the presence of an alteration coating (section 5.1), should be considered to explain the water contents variations.

[57] The presence of frost during winter could enrich the amount of adsorbed water through several possible micro-

physical mechanisms. First, adsorbed water is a more stable state than frost [*Möhlmann*, 2004]. Water molecules can therefore move from ice phase to adsorbed phase thanks to the direct contact of frost with minerals. Secondly, the presence of frost in winter maintains a high water vapor pressure in the neighborhood of the surface [*Böttger et al.*, 2005] and thus should also increase the amount of adsorbed water according to the isotherms of *Zent and Quinn* [1997] or the isobars of *Jänchen et al.* [2006]. A third possibility is described for instance by *Arvidson et al.* [2004]: the presence of frost could enable thin films of liquid water to develop at the surface of minerals and protect them. From these films water could adsorb on minerals.

[58] The sublimation of frost during spring is certainly not an instantaneous phenomenon because after winter, diurnal temperatures increase enough to be over the subli-

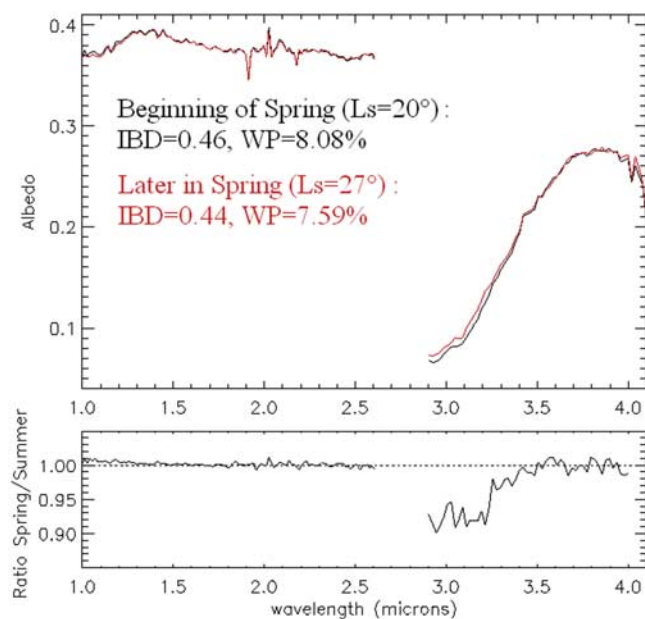


Figure 15. Albedo spectra of the point 48°N , -102°E observed at $L_s = 19.8^{\circ}$ (black curve, spring, orbit 305) and $L_s = 27.4^{\circ}$ (red curve, spring, orbit 357). IBD varies from 0.456 to 0.444; WP varies from 8.08% to 7.59%.

mation point, but night temperatures are cold enough to maintain frost during the night. The places we observe at the beginning of spring are depleted of frost at the time of observation but possibly not during the night, which maintains a high amount of adsorbed water on minerals. On the contrary summer observations correspond to places where frost is no more even during nighttime; therefore the averaged amount of adsorbed water has decreased compared to spring.

[59] This desorption phenomenon can bring new elements for the study of global water exchange. Linking the desorption phenomenon to the amount of water vapor in the atmosphere is difficult since other mechanisms occur, but the desorption process should be taken into account. TES results [Smith, 2006] show a small increase of the water vapor column during spring (from solar longitude about 45°) in the latitudes 40°N – 60°N . This increase occurs before the sublimation of the northern polar cap. It has been attributed to the sublimation of local frost, but it could also result from the desorption process as predicted by Titov [2002]. This TES observation is correlated to the OMEGA observation of the hydration seasonal variations from solar longitude 30° to 100° . At the end of spring the increase of water vapor column is very high in the considered latitudes [Smith, 2006; Encrenaz et al., 2005], resulting from the sublimation of the northern cap frost and diffusion to lower latitudes. The quantity of this kind of water vapor is expected to be much more important than the water vapor due to the mineral desorption phenomenon measured at 40°N – 60°N .

[60] Titov [2002] showed the importance of the regolith as a reservoir in the water cycle using numerical simulations and Viking orbiter observations. They deduced kinetics laws for the adsorption phenomenon and gave a first approximation of the amount of water stored in the regolith.

OMEGA observations of the $3\ \mu\text{m}$ band now give the possibility to observe these amounts directly.

6. Conclusions

[61] The reflectance spectra provided by the near-infrared imaging spectrometer OMEGA give the possibility to study the hydration of the Martian soils through the broad and deep absorption band at $3\ \mu\text{m}$. This band is assumed to be caused by the stretching and bending vibrations of the water molecule, present as adsorbed water (that is reversibly exchangeable with the atmosphere), structural water or metal-OH bonds. A specific data reduction tool has been developed to process the data from the channel $2.5\ \mu\text{m}$ – $5.1\ \mu\text{m}$. This tool includes thermal removal thanks to the assessment of the temperature of OMEGA I/F spectra at $5\ \mu\text{m}$. OMEGA reveals several important properties of the $3\ \mu\text{m}$ band.

[62] 1. The $3\ \mu\text{m}$ band is present everywhere on the Martian surface, suggesting it is caused by adsorbed water and maybe by an alteration layer containing structural water present all over the surface due to a long-term atmosphere/surface weathering.

[63] 2. Our measure of the surface hydration increases with albedo: even if an albedo dependence of the method cannot be excluded, a real increase of hydration with albedo is likely to occur since physical parameters connected to albedo such as grain size, composition or temperature must also influence the water content.

[64] 3. An increase of the $3\ \mu\text{m}$ band is observed in places where clays and sulfates have been observed, probably due to supplementary structurally adsorbed water in minerals. This observation shows that hydration at $3\ \mu\text{m}$ may detect remnant water from past alteration. This is also the first observation of band shape variation due to composition: the $3\ \mu\text{m}$ band is larger in sulfate minerals, suggesting variations in the energy bonds of water with minerals.

[65] 4. The $3\ \mu\text{m}$ band seems to decrease with altitude for low albedos, suggesting that the decrease of water vapor

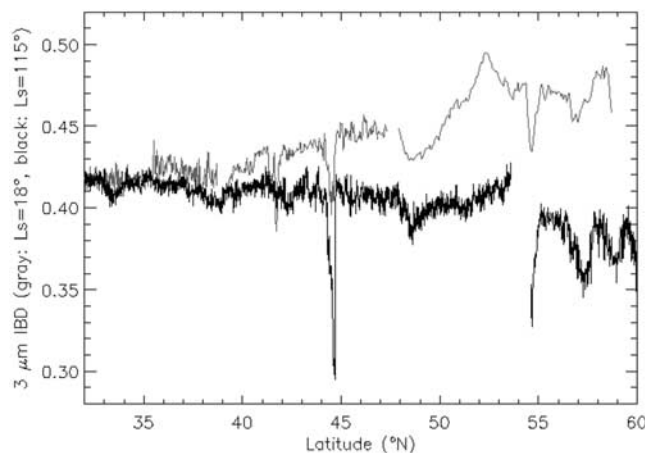


Figure 16. IBD versus latitude for two OMEGA overlapping orbits (longitude is 37°E), to illustrate the dehydration between spring and summer. Gray: IBD of spring track (orbit 294, $L_s = 18^{\circ}$). Black: IBD of summer track (orbit 1058, $L_s = 115^{\circ}$).

pressure enables less water to adsorb on minerals. This observation needs additional OMEGA data to get a more representative statistic sample. If proven to be real, this variation could help to better constrain the isotherms and isobars of adsorption on Mars. For high albedos no correlation is detected between hydration and altimetry, suggesting a permanent redistribution of dust all over the planet.

[66] 5. The temporal evolution of the 3 μm band has been shown in the 40°N–60°N latitudes between the beginning of spring and the beginning of summer. At the beginning of spring the hydration of the soils seems to increase with latitude. These two phenomena are best explained by the presence of frost in these places during winter, which enriches minerals in adsorbed water. When frost sublimates, soils come into balance with the atmosphere by releasing the adsorbed water toward the atmosphere. In parallel with this phenomenon temperature increases, lowering the adsorption capacity of minerals.

[67] The OMEGA instrument has been providing much more data than those that are studied. These supplementary data will be processed to extract the information about hydration once a new instrumental calibration adapted to these data is available.

References

- Anderson, D. M., and A. R. Tice (1979), The analysis of water in the Martian regolith, *J. Mol. Evol.*, *14*, 33–38.
- Arvidson, R. E., et al. (2004), Localization and physical properties experiments conducted by Spirit at Gusev Crater, *Science*, *305*, 821–824.
- Arvidson, R. E., et al. (2005), Spectral reflectance and morphologic correlations in eastern Terra Meridiani, Mars, *Science*, *307*, 1591–1594.
- Bibring, J.-P., et al. (1989), Results from the ISM experiment, *Nature*, *341*, 591–593.
- Bibring, J.-P., et al. (2004a), OMEGA: Observatoire pour la Minéralogie, l'Eau, les Glaces et l'Activité, in *Mars Express: The Scientific Payload*, edited by A. Wilson, *Eur. Space Agency Spec. Publ., ESA-1240*, 37–49.
- Bibring, J. P., et al. (2004b), Perennial water ice identified in the south polar cap of Mars, *Letters Nature*, *428*, 627–630.
- Bibring, J. P., et al. (2005), Mars surface diversity as revealed by the OMEGA/Mars Express observations, *Science*, *307*, 1576–1581.
- Biemann, K., J. Oro, P. Toulmin, L. E. Orgel, A. O. Nier, D. M. Anderson, D. Flory, A. V. Diaz, D. R. Rushneck, and P. G. Simmonds (1977), The search for organic substances and inorganic volatile compounds in the surface of Mars, *J. Geophys. Res.*, *82*, 4641–4658.
- Bish, D. L., J. W. Carey, D. T. Vaniman, and S. J. Chipera (2003), Stability of hydrous minerals on the Martian surface, *Icarus*, *164*, 96–103.
- Bishop, J. L., C. M. Pieters, and J. O. Edwards (1994), Infrared spectroscopic analyses on the nature of water in montmorillonite, *Clays Clay Miner.*, *42*, 702–716.
- Böttger, H. M., S. R. Lewis, P. L. Read, and F. Forget (2005), The effects of the Martian regolith on GCM water cycle simulations, *Icarus*, *177*, 174–189.
- Bruckenthal, E. A., and R. B. Singer (1987), Spectral effects of dehydration on phyllosilicates, *Proc. Lunar Planet. Sci. Conf. 18th*, 135.
- Calvin, W. M. (1997), Variation of the 3 μm absorption feature on Mars: Observations over eastern Valles Marineris by the Mariner 6 infrared spectrometer, *J. Geophys. Res.*, *102*, 9097–9107.
- Cooper, C. D., and J. F. Mustard (1999), Effects of very fine particle size on reflectance spectra of smectite and palagonitic soil, *Icarus*, *142*, 557–570.
- Encrenaz, T., et al. (2005), A mapping of Martian water sublimation during early northern summer using OMEGA/Mars Express, *Astron. Astrophys.*, *441*, L9–L12.
- Erard, S., and W. Calvin (1997), New composite spectra of Mars, 0.4–5.7 mm, *Icarus*, *130*, 449–460.
- Farmer, C. B., D. W. Davies, and D. D. Laporte (1976), Mars: Northern summer ice CAP—Water vapor observations from Viking 2, *Science*, *194*, 1339–1341.
- Feldman, W. C., et al. (2004), Global distribution of near-surface hydrogen on Mars, *J. Geophys. Res.*, *109*, E09006, doi:10.1029/2003JE002160.
- Fialips, C. I., J. W. Carey, and D. L. Bish (2004), Hydration-dehydration behavior and thermodynamics of chabazite, *Geochim. Cosmochim. Acta*, *69*, 2293–2308.
- Foley, C. N., T. Economou, and R. N. Clayton (2003), Final chemical results from the Mars Pathfinder alpha proton X-ray spectrometer, *J. Geophys. Res.*, *108*(E12), 8096, doi:10.1029/2002JE002019.
- Forget, F., F. Hourdin, R. Fournier, C. Hourdin, O. Talagrand, M. Collins, S. R. Lewis, P. L. Read, and J.-P. Huot (1999), Improved general circulation models of the Martian atmosphere from the surface to above 80 km, *J. Geophys. Res.*, *104*, 24,155–24,176.
- Gendrin, A., et al. (2005), Sulfates in Martian layered terrains: The OMEGA/Mars Express view, *Science*, *307*, 1587–1591.
- Gondet, B., J.-P. Bibring, Y. Langevin, F. Poulet, F. Montmessin, and F. Forget (2006), One Martian year observation of H₂O ice clouds By OMEGA/Mars Express, paper presented at Second Workshop on Mars Atmosphere Modelling and Observations, Cent. Natl. d'Etudes Spatiales, Granada, Spain.
- Hapke, B. (1993), *Theory of Reflectance and Emittance Spectroscopy*, 455 pp., Cambridge Univ. Press, New York.
- Hecht, M. H. (2002), Metastability of liquid water on Mars, *Icarus*, *156*, 373–386.
- Huwot, J. A., S. M. McLennan, N. J. Tosca, R. E. Arvidson, J. R. Michalski, D. W. Ming, C. Schröder, and S. W. Squyres (2006), In situ and experimental evidence for acidic weathering of rocks and soils on Mars, *J. Geophys. Res.*, *111*, E02S19, doi:10.1029/2005JE002515.
- Jänchen, J., D. L. Bish, D. T. Möhlmann, and H. Stach (2006), Investigation of the water sorption properties of Mars-relevant micro- and mesoporous minerals, *Icarus*, *180*, 353–358.
- Langevin, Y., F. Poulet, J.-P. Bibring, B. Schmitt, S. Douté, and B. Gondet (2005a), Summer evolution of the north polar cap of Mars as observed by OMEGA/Mars Express, *Science*, *307*, 1581–1584.
- Langevin, Y., F. Poulet, J.-P. Bibring, and B. Gondet (2005b), Sulfates in the north polar region of Mars detected by OMEGA/Mars Express, *Science*, *307*, 1584–1586.
- Lewis, S. R., M. Collins, P. L. Read, F. Forget, F. Hourdin, R. Fournier, C. Hourdin, O. Talagrand, and J.-P. Huot (1999), A climate database for Mars, *J. Geophys. Res.*, *104*, 24,177–24,194.
- Melchiorri, R., P. Drossart, T. Fouchet, B. Bézart, F. Forget, A. Gendrin, J. P. Bibring, N. Manaud, and Omega Team (2006), A simulation of the OMEGA/Mars Express observations: Analysis of the atmospheric contribution, *Planet. Space Sci.*, *54*, 774–783.
- Milliken, R. E., and J. F. Mustard (2005), Quantifying absolute water content of minerals using near-infrared reflectance spectroscopy, *J. Geophys. Res.*, *110*, E12001, doi:10.1029/2005JE002534.
- Milliken, R. E., J. F. Mustard, F. Poulet, D. Jouglet, J.-P. Bibring, B. Gondet, and Y. Langevin (2007), Hydration state of the Martian surface as seen by Mars Express OMEGA: 2. H₂O content of the surface, *J. Geophys. Res.*, doi:10.1029/2006JE002853, in press.
- Möhlmann, D. T. (2004), Water in the upper Martian surface at mid- and low-latitudes: Presence, state, and consequences, *Icarus*, *168*, 318–323.
- Murchie, S., J. Mustard, J. Bishop, J. W. Head, C. Pieters, and S. Erard (1993), Spatial variations in the spectral properties of bright regions on Mars, *Icarus*, *105*, 454–468.
- Mustard, J. F., F. Poulet, A. Gendrin, J.-P. Bibring, Y. Langevin, B. Gondet, N. Mangold, G. Bellucci, and F. Altieri (2005), Olivine and pyroxene diversity in the crust of Mars, *Science*, *307*, 1594–1597.
- Picardi, G., et al. (2005), Radar soundings of the subsurface of Mars, *Science*, *310*, 1925–1928.
- Pimentel, G. C., P. B. Forney, and K. C. Herr (1974), Evidence about hydrate and solid water in the Martian surface from the 1969 Mariner Infrared Spectrometer, *J. Geophys. Res.*, *79*, 1623–1634.
- Poulet, F., J. P. Bibring, J. F. Mustard, A. Gendrin, N. Mangold, Y. Langevin, R. E. Arvidson, B. Gondet, and C. Gomez (2005a), Phyllosilicates on Mars and implications for early Martian climate, *Nature*, *438*, 623–628.
- Poulet, F., Y. Langevin, J.-P. Bibring, B. Gondet, R. E. Arvidson, and Omega Team (2005b), Mineralogy of the northern high latitude regions of Mars, *Lunar Planet. Sci.*, *XXXVI*, Abstract 1828.
- Poulet, F., C. Gomez, J.-P. Bibring, Y. Langevin, B. Gondet, P. Pinet, G. Bellucci, and J. Mustard (2007), Martian surface mineralogy from Observatoire pour la Minéralogie, l'Eau, les Glaces et l'Activité on board the Mars Express spacecraft (OMEGA/MEx): Global mineral maps, *J. Geophys. Res.*, *112*, E08S02, doi:10.1029/2006JE002840.
- Richard, T., L. Mercury, F. Poulet, and L. d'Hendecourt (2006), Diffuse reflectance infrared Fourier transform spectroscopy as a tool to characterize water in adsorption/confinement situations, *J. Colloid Interface Sci.*, *304*, 125–136.
- Richardson, M. I., and M. A. Mischna (2005), Long-term evolution of transient liquid water on Mars, *J. Geophys. Res.*, *110*, E03003, doi:10.1029/2004JE002367.
- Ruff, S. W. (2004), Spectral evidence for zeolite in the dust on Mars, *Icarus*, *168*, 131–143.
- Schmitt, B., S. Douté, Y. Langevin, F. Forget, J.-P. Bibring, G. Bellucci, F. Altieri, F. Poulet, and B. Gondet (2005), Spring sublimation of the

- seasonal condensates on Mars from OMEGA/Mars Express, *Eos Trans. AGU*, 86(52), Fall Meeting Suppl., Abstract P23C-02.
- Smith, M. D. (2004), Interannual variability in TES atmospheric observations of Mars during 1999–2003, *Icarus*, 167, 148–165.
- Smith, M. D. (2006), TES atmospheric, aerosol optical depth, and water vapor observations 1999–2004, paper presented at Second Workshop on Mars Atmosphere Modelling and Observations, Cent. Natl. d'Etudes Spatiales, Granada, Spain.
- Smith, M. D., et al. (2004), First atmospheric science results from the Mars Exploration Rovers Mini-TES, *Science*, 306, 1750–1753.
- Squyres, S. W., et al. (2004), In situ evidence for an ancient aqueous environment at Meridiani Planum, Mars, *Science*, 306, 1709–1714.
- Svitek, T., and B. Murray (1990), Winter frost at Viking Lander 2 site, *J. Geophys. Res.*, 95, 1495–1510.
- Titov, D. V. (2002), Water vapour in the atmosphere of Mars, *Adv. Space Res.*, 29, 183–191.
- Vaniman, D. T., D. L. Bish, S. J. Chipera, C. I. Fialips, J. W. Carey, and W. C. Feldman (2004), Magnesium sulphate salts and the history of water on Mars, *Nature*, 431, 663–665.
- Yen, A. S., B. C. Murray, and G. R. Rossman (1998), Water content of the Martian soil: Laboratory simulations of reflectance spectra, *J. Geophys. Res.*, 103, 11,125–11,133.
- Yen, A. S., et al. (2005), An integrated view of the chemistry and mineralogy of Martian soils, *Nature*, 435, 49–54.
- Zent, A. P., and R. C. Quinn (1995), Simultaneous adsorption of CO₂ and H₂O under Mars-like conditions and application to the evolution of the Martian climate, *J. Geophys. Res.*, 100, 5341–5349.
- Zent, A. P., and R. C. Quinn (1997), Measurement of H₂O adsorption under Mars-like conditions: Effects of adsorbent heterogeneity, *J. Geophys. Res.*, 102(E4), 9085–9095.
-
- J.-P. Bibring, C. Gomez, B. Gondet, D. Jouglet, Y. Langevin, and F. Poulet, Institut d'Astrophysique Spatiale (IAS), Université Paris 11, Bâtiment 121, F-91405 Orsay Cedex, France. (denis.jouglet@ias.u-psud.fr)
R. E. Milliken and J. F. Mustard, Department of Geological Sciences, Brown University, Providence, RI 02912, USA.